Nanostructured Pt-alloy electrocatalysts for PEM fuel cell oxygen reduction reaction

Bing, Yonghong; Liu, Hansan; Zhang, Lei; Ghosh, Dave; Zhang, Jiujun

Publisher's version / Version de l'éditeur:
https://doi.org/10.1039/b912552c
Chemical Society Reviews, 39, 6, pp. 2184-2202, 2010-03-25

Nanostructured Pt-alloy electrocatalysts for PEM fuel cell oxygen reduction reaction

Yonghong Bing, Hansan Liu, Lei Zhang, Dave Ghosh and Jiujun Zhang*

Received 25th June 2009
First published as an Advance Article on the web 25th March 2010
DOI: 10.1039/b912552c

In this *critical review*, we present the current technological advances in proton exchange membrane (PEM) fuel cell catalysis, with a focus on strategies for developing nanostructured Pt-alloys as electrocatalysts for the oxygen reduction reaction (ORR). The achievements are reviewed and the major challenges, including high cost, insufficient activity and low stability, are addressed and discussed. The nanostructured Pt-alloy catalysts can be grouped into different clusters: (i) Pt-alloy nanoparticles, (ii) Pt-alloy nanotextures such as Pt-skins/monolayers on top of base metals, and (iii) branched or anisotropic elongated Pt or Pt-alloy nanostructures. Although some Pt-alloy catalysts with advanced nanostructures have shown remarkable activity levels, the dissolution of metals, including Pt and alloyed base metals, in a fuel cell operating environment could cause catalyst degradation, and still remains an issue. Another concern may be low retention of the nanostructure of the active catalyst during fuel cell operation. To facilitate further efforts in new catalyst development, several research directions are also proposed in this paper (130 references).

1. Introduction

The high cost of proton exchange membrane (PEM) fuel cell technology is one of the major challenges hindering its commercialization. Among the components in a PEM fuel cell, platinum (Pt)-based electrocatalysts and their associated catalyst layers contribute over 55% of the total cost.[1,2] Unfortunately, Pt-based catalysts are currently the only choice of electrocatalysts in practical PEM fuel cells. Because the dominant polarization in a PEM fuel cell comes from the slow cathodic oxygen reduction reaction (ORR) rather than the anodic hydrogen oxidation reaction, reducing the Pt loading (particularly in the cathode catalyst layer) without compromising fuel cell performance is an effective strategy to meet the cost requirements for fuel cell commercialization.[3–5] In other words, the design of novel catalysts requires not only reducing the amount of Pt used but also enhancing catalytic activity and stability.[6] In order to address these requirements, several approaches have been developed, including (i) making nanostructures to increase the surface-to-volume ratio;[7] (ii) using an alloying technique to incorporate non-precious metals into the nanostructures; and (iii) texturing nanostructures, for

Institute for Fuel Cell Innovation, National Research Council of Canada, Vancouver, Canada BC V6T 1W5.
E-mail: jiujun.zhang@nrc.gc.ca; Tel: 604-221-3087

Yonghong Bing

Dr Yonghong Bing received her PhD from Simon Fraser University in 2005 in inorganic chemistry. She won one of the two Doctoral Prizes in engineering and computer sciences from Natural Sciences and Engineering Research Council of Canada (NSERC) in 2006. She then joined University of Washington as an NSERC postdoctoral fellow in 2006. She came to the National Research Council of Canada Institute for Fuel Cell Innovation as a Research Associate in 2008. Her research interests include functional nanostructured materials, fuel cell catalysts, battery and supercapacitor materials, solid-state chemistry and crystalline materials for electronic and clean energy applications.

Hansan Liu

Dr Hansan Liu is a Research Associate at the National Research Council of Canada Institute for Fuel Cell Innovation. He obtained his PhD in electrochemistry from Xiamen University in 2003. Dr Liu has over ten years of research experience in the field of electrochemical energy conversion and storage. His current research interests include fuel cell electrocatalysis, battery and supercapacitor materials, and aerosol techniques for nanomaterial synthesis. He has published over forty papers in peer-reviewed journals, co-edited a fuel cell book, and written four book chapters relating to fuel cells and batteries. He also has three US patent applications and eight industrial technical reports to his name.

example, replacing the core atoms in Pt nanoparticles with a non-precious metal, resulting in a Pt-skin[8,9] or Pt monolayer on top of catalysts.[10–12] In each such approach, the effects of shape (zero-, one-, two- or three-dimensional nanostructures), morphology (exposed facets), and catalyst composition on electrocatalytic activity and stability should be considered.[13–16] In synthesis processes, optimizing catalyst shape, morphology and composition with respect to catalytic activity and stability is critical to achieve successful electrocatalysts.

In the past several decades, significant effort has been put into the design and synthesis of Pt nanostructures for PEM fuel cell catalysts to increase their catalytic activity and stability. Research groups worldwide have reported successes, such as: (i) simply alloying Pt with the second transition metals,[17–21] (ii) textured Pt-alloys with core–shell structures,[22–24] (iii) morphology-controlled large Pt-alloy crystals,[8,25] and (iv) elongation of shape-controlled Pt-alloy in at least one dimension.[15,26–28] Gasteiger and Marković[29] recently reported on the incremental progress that has been made in improving ORR performance in PEM fuel cells *via* revolutionizing the Pt-based catalyst nanostructure, as shown in Fig. 1. In this image, the catalytic activity (AC) for the ORR is expressed by the concept of turnover frequency (TOF), which can be related to the ORR current density (I, C s^{-1} cm^{-3}) at a certain electrode potential, to the electron charge (*i.e.*, 1.6×10^{-19} C), and to the active site density (ASD, site cm^{-3}) by the equation: TOF = I/(e ASD). Here, TOF has a unit of e $site^{-1}$ s^{-1}. At the current stage of research and development, the best practical catalysts in PEM fuel cell are Pt nanoparticles with a thermodynamically spherical shape enclosed by low-index facets, which have a TOF of 25 e $site^{-1}$ s^{-1}. Fig. 1 shows that the best TOF achieved was as high as 2800 e $site^{-1}$ s^{-1}, obtained from $Pt_3Ni\{111\}$ nanocrystals with a highly structured

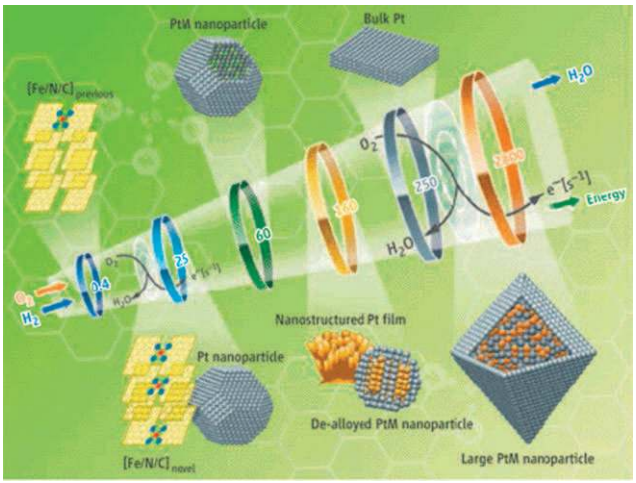

Fig. 1 Incremental progress in the electrochemical conversion of oxygen and hydrogen to energy and water in a PEM fuel cell, in terms of turnover frequencies. (Operating conditions: 80 °C, 100 kPa_{abs} H_2 and O_2, at 0.8 V *vs.* RHE). (Reprinted from ref. 29 with permission by the American Association for the Advancement of Science.)

Lei Zhang

Ms Lei Zhang is a Research Council Officer at National Research Council of Canada Institute for Fuel Cell Innovation. She received her first MSc majoring in Inorganic Chemistry from Wuhan University in 1993, and her second MSc in Materials Chemistry from Simon Fraser University in 2000. Ms. Zhang's main research interests include PEM fuel cell electrocatalysis, catalyst layer/electrode structure and metal–air batteries/fuel cells. She has co-authored over thirty journal papers and holds five US patent applications. Ms Zhang is an adjunct Professor of Federal University of Maranhao, Brazil, and an active member of the Electrochemical Society and the International Society of Electrochemistry.

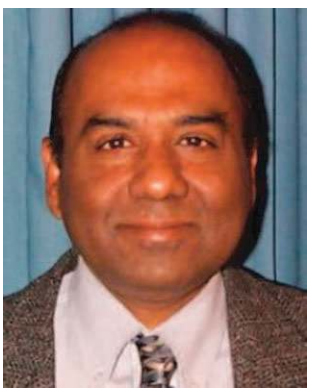

Dave Ghosh

Dr Dave Ghosh joined the National Research Council in September of 2002 as the Director of Science and Technology. He leads a team of over 85 researchers and engineers working in PEM fuel cells, SOFC and Hydrogen technologies. Before joining the NRC IFCI, Dave Ghosh was VP and CTO for Calgary-based Global Thermoelectric Inc. (presently Versa Power Systems) where he helped turn the company into one of the world's leading developers of Solid Oxide Fuel Cell Systems. Dave has held industrial R&D positions in Japan, Brazil and Canada. Dave has a PhD in Materials Science and Engineering from McMaster University, Hamilton, Canada. He has published over 60 technical papers and has co-authored over 11 patents granted.

Jiujun Zhang

Dr Jiujun Zhang received his BSc and MSc from Peking University in 1982 and 1985, respectively, and his PhD from Wuhan University in 1988, all in Electrochemistry and now he is a Senior Research Officer and PEM Catalysis Core Competency Leader at the National Research Council of Canada Institute for Fuel Cell Innovation (NRC-IFCI). Dr Zhang holds several adjunct professorships, including one at the University of Waterloo and one at the University of British Columbia. His research is mainly based on fuel cell catalysis development. Dr Zhang is also an active member of The Electrochemical Society, the International Society of Electrochemistry, and the American Chemical Society.

compositional oscillation in the near-surface layers. Although it is extremely difficult to achieve such a high TOF in a fuel cell operation environment, there is plenty of room for improving catalyst activity in such an environment by exploring Pt-alloy catalysts with novel, stable nanostructures.

It is generally recognized that the sluggish kinetics associated with the ORR at a PEM fuel cell cathode when the reaction is catalyzed by Pt-based catalysts can lead to high overpotential, resulting in low performance. To further improve catalyst activity, another theoretical approach, apart from the catalyst designs and synthesis mentioned above, is to develop new catalysts. With this in mind, researchers have given considerable attention in recent years to developing a fundamental understanding of the ORR mechanism catalyzed by Pt-based catalysts. For example, Filhol and Neurock[30] carried out theoretical calculations using a periodic density function method to determine the potential dependency of the reaction energy and activation barrier for the first reduction step of adsorbed molecular oxygen, this first reduction step being recognized as the rate-determining step in the ORR. First-principle analysis by the same research group[31] recently pointed out that on a fully hydrated Pt(111) surface, electron transfer precedes protonation of the absorbed O_2 molecule. Through a pattern of hydrogen bonding, the proton is bound to the adsorbed O_2 molecule in the form of H_3O^+. The group's results were applied to explain the initial stages of O_2 adsorption and activation as a function of applied potential on well-defined Pt and Pt-skin alloys, and were validated by experimental results.[32] A review in 2008 by Nørskov *et al.*[33] explained fundamental concepts such as "Brønsted–Evans–Polanyi relations" and "volcano curves," and employed these concepts to explain the catalytic activity of Pt-alloys. Discussing how catalytic activity is affected by the electronic structure of the catalyst and geometric distribution, they also emphasized a strict partitioning between "electronic" and "geometrical" effects. In this article, Nørskov *et al.* assigned the d-band center—the first moment of the density of states projected onto the d-orbital for the surface atoms interacting with the adsorbate—as a measure of the ability of an atom to form bonds with an adsorbate. They concluded that late transition metal atoms with low coordination numbers (*i.e.*, having open surfaces, steps, edges, kinks and corners) tend to have higher d-states and therefore interact more strongly with adsorbates than do the atoms on close-packed surfaces with high metal coordination numbers. This theory, which has been experimentally validated by Stamenkovic *et al.*[34] and successfully applied in the search for ORR catalysts more effective than Pt, shows that Pt-alloys involving 3d metals are better catalysts than Pt because the electronic structure of Pt atoms on the surface of Pt-alloys has been slightly modified. Stamenkovic *et al.* developed a series of well-characterized alloys that showed interesting volcano-shaped variations in electrocatalytic activity, and provided a starting point for developing and understanding the factors that control ORR kinetics. The calculation by Stamenkovic and Nørskov *et al.* concluded that oxygen molecules adsorbed on a Pt(111) electrode tend to be so stable at high potentials that proton and electron transfers become impossible, suggesting a reason for the overpotential of Pt catalysts. Lowering the binding energy could make the oxygen on a Pt surface less stable and thereby accelerate the reaction.[35]

It is currently believed that novel catalyst synthesis strategies are essential to develop effective Pt-based catalysts for PEM fuel cell applications. In this paper, three aspects of catalyst technology development for the ORR in PEM fuel cells are reviewed, according to catalyst nanostructures: (i) Pt-alloy nanoparticles, (ii) Pt-alloy nanotextures, such as Pt-skins/monolayers on top of base metals, and (iii) branched or anisotropic elongated Pt- or Pt-alloy nanostructures. Scheme 1 presents the construction of this paper aligning with the research trend in development of effective Pt-based catalysts for PEM fuel cell ORR application. In addition, the activity and stability of presently developed nanostructured catalysts will also be reviewed.

2. Pt-alloy nanoparticles—the thermodynamically favoured spherical shape

2.1 Current status—geometric and compositional strategies

Platinum has a face-centered cubic (fcc) crystal structure with a lattice parameter of 3.93 Å. The surface energies (γ) of the low-index crystallographic planes are in the order of $\gamma(111) < \gamma(100) < \gamma(110)$.[36,37] The commonly observed Pt nanoparticles are in the thermodynamically favoured spherical shape, enclosed by low-index facets, such as Pt{100} and Pt{111}. In terms of catalytic activity, the nanosized Pt catalyst offers several advantages, including larger surface to volume ratio,[38] increased Pt utilization, and a greater number of available catalytic sites as compared with Pt bulk single crystals. These advantages make it the most active catalyst for many electrochemical reactions, including both oxygen reduction and hydrogen oxidation in fuel cells. In general, the intrinsic reactivity and selectivity of Pt catalysts are controlled by the crystalline structures and morphologies of the particles. Therefore, different facets on Pt nanoparticles have different catalytic activities towards fuel cell reactions. This is probably due to the distinct adsorption properties of the different chemical species on these facets.

Feliu and co-workers[39,40] intensively studied the effect of surface orientation of single Pt crystals on ORR electron transfer, and concluded that the ORR is actually a structure-sensitive reaction in both sulfuric and perchloric media. The orientation of the steps and terraces on the surface plays a significant role in determining the electrocatalytic activity of an electrode. Experimental results confirmed that in an ORR electrocatalyzed by Pt catalyst, if H_2SO_4 is being used as an electrolyte, Pt{100} presents a higher ORR activity than Pt{111}. This was found to be due mainly to the adsorption and inhibiting effects of the bisulfate anion.[41] Regarding the effect of electrolyte ions on the catalytic activity of Pt facets, systematic investigations of the adsorption of bisulfate anions have been carried out by Zelenay *et al.*,[42] Varga *et al.*,[43] and Gamboa-Aldeco *et al.*[44] Their studies showed that bisulfate coverage on a Pt(100) electrode was less than one-third of the coverage on a Pt(111) electrode in the same concentration of sulfuric acid solution. Pt(111) can adsorb bisulfate anions much more strongly and in a wider potential range than Pt(100), due to the different properties of their respective facets. However, this seems not to be so when $HClO_4$ is used

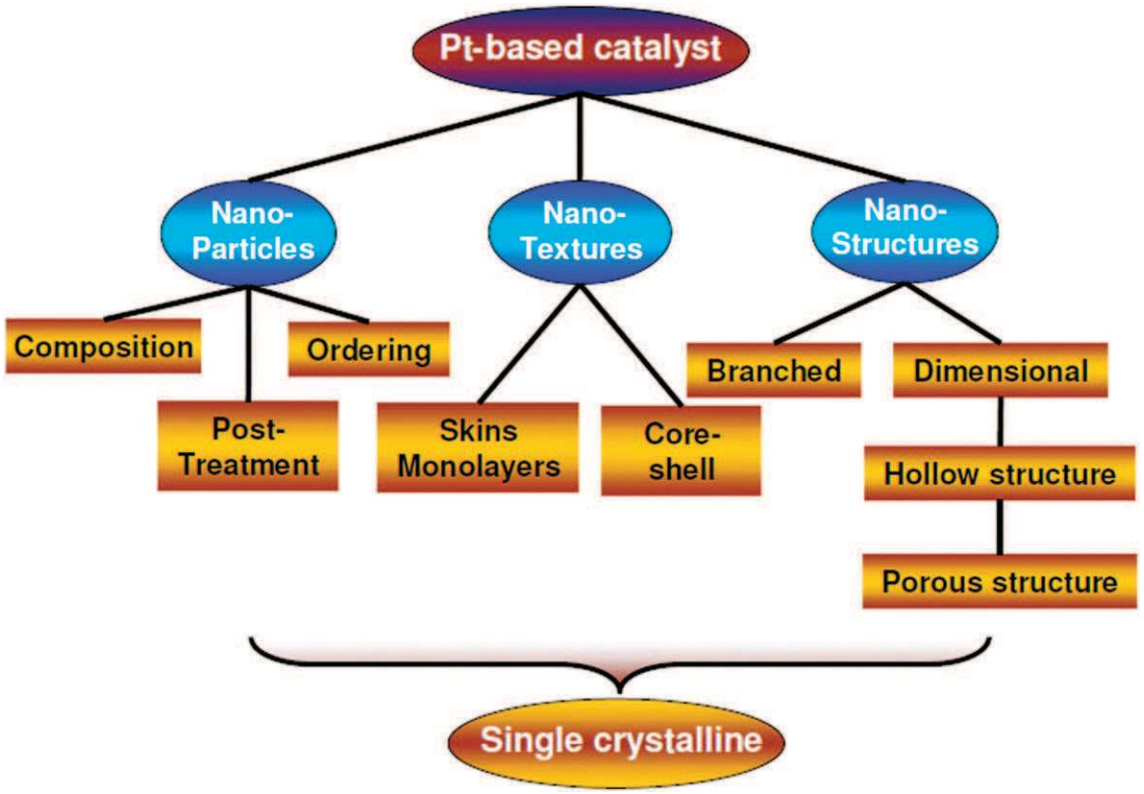

Scheme 1 Schematic representation of the research trend in the development of effective Pt-based catalysts for PEM fuel cell applications.

as an electrolyte; in this case, the catalytic activity increases thus: Pt{110} > Pt{111} > Pt{100}. This finding was determined to be the result of selective interaction between O_2 and different exposed facets, as well as increased adsorption of the OH species on these Pt surfaces.[8] Armand and Clavilier[45,46] investigated the influence of specific anion adsorption on the electrochemical behavior of Pt(100), (110) and (111) surfaces in an acidic medium, carrying out voltammetric cycling in both sulfuric and perchloric acid solutions and using hydrogen as a structure-sensitive probe. They showed that the atomic surface structure of Pt(100) and (110) facets underwent reconstruction during electrode cycling, resulting in a more stable and densely packed surface structure. However, this did not occur for Pt(111). They concluded that the surface modification experienced by the (100) and (110) orientations after electrode cycling in the potential range where specific adsorption occurred resulted from the specific adsorption of anions. There was no evidence to indicate any structural transition between Pt(100) and (110) after electrochemical treatment.

Controlling the synthesis process to produce favoured catalyst morphologies, including surface structures with designed crystal facets, thus seems quite important in creating highly active, Pt-based catalysts. It is worth emphasizing that some specially featured crystal facets (high-index facets, facets with terraces) on the catalyst surface play a major role in catalytic activity enhancement because they offer a greater number of active sites located at edges or corners of the rough surface of the Pt particles.[47–49] Wang *et al.*[50] demonstrated that a Pt nanocube catalyst was four times more active in 0.5 M H_2SO_4 than a Pt nanoparticle, in terms of ORR specific activity. This might be due to the high exposure of the Pt{100} facets, which may provide optimal binding energy between platinum atoms and the adsorbed species for ORR.[51] Furthermore, some nanostructures enclosed within high-index facets could contain more unsaturated atomic steps, edges and kinks, which are believed to be more catalytically active than the commonly formed nanostructures within low-index facets.[15,37,52] Tian *et al.*[53] reported Pt tetrahexahedra with exposed high-index planes (*e.g.* {730}, {210} and {520} facets), which exhibited 2–4 times more efficiency per unit surface area for ethanol oxidation compared to a commercially available Pt/C catalyst, that is usually enclosed with low-index planes such as {111} and {100}.

However, the surface structure of such nanoparticles can be unstable during PEM fuel cell reactions, especially those with high-index planes and unsaturated atomic steps, edges and kinks, all of which are active sites for crystal growth. Due to the morphological changes that Pt nanoparticles undergo during fuel cell operation, these facets may easily be deactivated, resulting in degradation of their catalytic activity. Alloying Pt with some relatively small base metals has the advantages of reducing the amount of Pt used, while at the same time improving activity and stability as compared to pure Pt catalysts.[3,54,55] It has been demonstrated that when Pt is alloyed with Cr, Mn, Fe, Co and Ni, a two- to four-fold improvement in ORR specific activity ($\mu A\ cm^{-2}_{Pt}$), compared with a Pt catalyst, could be achieved.[19] The mechanisms for such enhanced activity have been investigated intensively and reviewed in the literature, with the result that changes in

surface electronic structure and adsorption properties after Pt alloying have been identified as reasons for the enhancement.[56–58] Nørskov *et al.*[35] studied nanoscale effects on electrocatalytic activity using density functional theory (DFT) calculations and showed that alloys of Pt and, for example, Ni, Co, Fe and Cr (where Pt is segregated on the surface) have smaller oxygen binding energies than pure Pt. Their results provided good explanations for experimental observations that the Pt skins on these alloys have higher catalytic activity than pure Pt.

Unfortunately, leaching or dissolution of the base metal from the alloy surface to the acidic solution has been identified as the major cause of catalyst deactivation. Therefore, some treatment of the Pt-alloy catalyst is necessary to improve its stability.

2.2 Effects of composition, structure, morphology and particle size on ORR electrocatalysis

As discussed above, one important strategy to reduce the use of Pt without compromising ORR activity and stability is to alloy Pt with other transition metals. In the past several decades, this strategy has proven very efficient in reducing noble metal use, as well as enhancing catalytic activity and stability. It has been demonstrated that Pt-alloys can achieve at least two to four times greater ORR activity compared to Pt/C catalysts.[3] This improvement was attributed to a positive shift of onset potential for OH_{ads} formation on the alloy. The major factors affecting ORR activity have been identified as alloy composition, ordering and morphology (the ratio of exposed facets), and the interactions among these factors. In the following sections, these factors and their interactions will be individually reviewed.

2.2.1 Effects of composition. Many carbon-supported Pt-alloy catalysts (PtM/C, M = Co,[18,59] Ni,[60] V,[61] Fe,[62–64] Cu,[59] Cr,[65] Mn,[19] Au,[66] Ir,[67] and so on) have been successfully synthesized. In earlier research stages, the primary efforts were put into investigating the effects of the Pt-alloy components and their compositions on ORR activity and stability, using a conventional Pt/C catalyst as the baseline; here, "components" refers to the choice of various base metals, while "compositions" refers to the ratio of Pt to base metal. For example, studies of ORR activity on PtM alloys (M = Ni, V, Co and Fe) revealed the following order of increasing activity: Pt/C < PtNi/C < PtV/C < PtCo/C < PtFe/C.[54,55,63]

Most Pt-alloys, regardless of the ratio between the noble metal and the base metal (*e.g.*, Pt_3Co/C, Pt_3Ni/C, Pt_1Ni_1/C, Pt_1Co_1/C, Pt_1Fe_1/C and PtV/C), displayed better stability than the baseline Pt/C.[63] However, the stability of Pt-alloys was proven to vary between the different base metals. Pt alloyed with Cr and Ti showed much more stable performance than the Fe, V and Ni alloys. One possible explanation for such a difference is that both Cr and Co may exhibit a higher degree of alloying with Pt than Fe, V and Ni, modifying the intrinsic catalytic activity by forming stronger Pt–Cr and Pt–Co bonds, and resulting in higher stability in an acidic medium.[55,63] In durability testing, both Pt/C and Pt-alloys/C showed a decline in catalytic activity, but the Pt-alloys/C had a much better retention time. One of the mechanisms for such degradation could be growth of the nanoparticles under extensive potential cycling, resulting in electrochemical surface area (ECSA) loss. To explore this possibility, investigations into activity loss in both Pt and PtCo alloy systems were carried out using potential cycling between 0.6–1.2 V *vs.* RHE; this work revealed up to a five-fold increase in Pt particle size from the beginning to the end of the testing, while very little change was found in the particle size of the PtCo alloy (Fig. 2).[68]

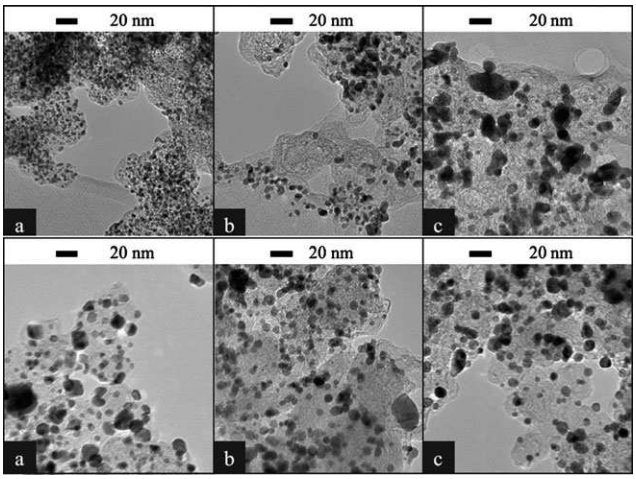

Fig. 2 TEM images of 60% Pt/C (top) and 40% PtCo/C (bottom): (a) before potential cycling, (b) after cycling at 0.6–1.0 V, and (c) after cycling 0.6–1.2 V. (Reproduced from ref. 69 by permission of ECS—The Electrochemical Society.)

To examine the effects of atomic ratios (*i.e.*, Pt to base metals), the fuel cell activity and stability of PtM/C (M = Co, Cr, Fe, Ni and Mn) have been studied; it was found that PtM alloys with a 3 : 1 Pt : M ratio exhibited much higher activity and better stability.[69,70] For example, comparison stability tests on a single fuel cell with Pt/C and Pt_3Co/C as cathode catalysts showed that the latter had greater stability. The degradation rate for Pt/C was 0.98 mV h^{-1}, twice that of Pt_3Co/C (0.44 mV h^{-1}).[55] Stability testing of Pt_3M alloys in a vacuum (M = Ir, Co, Ni and Fe) showed that $Pt_3Ir(111)$ > $Pt_3Co(111)$ > $Pt_3Ni(111)$ > $Pt_3Fe(111)$.[6]

Stamenkovic *et al.*[34] studied polycrystalline alloy films of Pt_3M catalysts (M = Ni, Co, Fe and Ti) to understand the role of 3d metals in the electrocatalytic ORR activity of Pt-alloys. They found that in these Pt_3M alloys, the first outlayer was enriched by Pt due to surface segregation. This Pt overlayer structure was found to be fairly stable in 0.1 M $HClO_4$ solution, and the catalytic activity for the ORR on such alloys was dependent on the nature of the 3d metal. While the Ni, Co and Fe alloys were much more active than pure Pt, alloys of the earlier 3d metals exhibited less enhancement. Fig. 3 shows catalytic activity *vs.* d-band center position at 0.9 V, and presents a classic volcano-shaped dependency. The study showed that the mechanism was either O_2 dissociation or proton/electron transfer to molecular O_2. Based on their model, a better ORR electrocatalyst should bind oxygen molecules more weakly than does Pt, to increase the removal rate of adsorbed O and OH species.

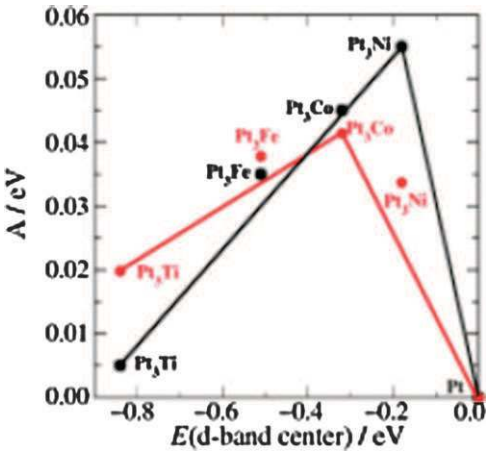

Fig. 3 Electrocatalytic activities *vs.* the experimentally measured d-band center relative to platinum. The activity predicted from DFT simulations is shown in black, and the measured activity is shown in grey. (Reprinted from ref. 34 with permission by Wiley-VCH Verlag GmbH & Co. KGaA.)

The drawbacks of Pt-alloys/C are dissolution of the transition metals into the PEM membrane electrode assembly (MEA) of the fuel cell, resulting in severe ion contamination. There is evidence to show that the degree of dissolution depends on both the particular base metal and the atomic ratio. For example, both Co and Fe are more easily dissolved in acidic solution. Increasing the base metal content in Pt-alloys may result in a large amount of dissolved base metal in the solution. Antolini *et al.*[55] investigated the relationship between the stability of the second metal and its content in the alloy, using $Pt_{1-x}M_x$ (M = Fe, Ni and Co), and revealed that when x was small, only the unalloyed base metal could be dissolved. However, if x was increased to 0.6, even an alloyed metal could be dissolved from the bulk alloy.[55,71] Some methods to address the base metal dissolution issue have been explored, including treating the as-prepared catalysts with acid or high temperatures to reduce the effect of unalloyed base metals.

2.2.2 Effects of post-treatments. As discussed above, unalloyed base metals on the surface layer of alloys are more easily dissolved in the reaction media.[72] To reduce the dissolution of base metals, post-treatment of alloys using chemical leaching or heat has been explored. These post-treatments have proven effective in improving both activity and stability, because the most unalloyed or unstable metal ions on the surface are either leached out by acid or further alloyed at high temperatures. For example, pre-leaching of PtCo alloys can effectively reduce Co dissolution and then minimize MEA contamination during PEM fuel cell operation.[3,73]

Roques *et al.*[74] studied on enhancing PtCo/C alloy catalyst stability by chemical acid leaching, using Pt/C as the baseline in their work. The catalyst was soaked in 1 M $HClO_4$ for 48 h at room temperature. Then both acid-washed and unwashed samples were examined by X-ray absorption near-edge structure (XANES) under a potential of 0.9 V *vs.* RHE. The results indicated that the acid-washed sample was more stable than the unwashed sample at 0.9 V for 6–10 h of testing, evidenced by the surface oxidation environment around Co remaining unchanged for acid-washed samples but changing for unwashed samples after stability testing. Interestingly, the Pt content remained unchanged for both washed and unwashed alloys throughout the tests.

Zhang *et al.*[75] and Bezerra[76] have extensively reviewed the effects of heat treatment on the catalytic activity and stability of various PEM fuel cell catalysts, including Pt alloys. They concluded that heat treatment could affect many characteristics, such as particle size, morphology and dispersion of metal on support, alloying degree, active site formation, as well as catalytic activity/stability. Heat treatment can give rise to a high degree of alloying and of crystalline structures; at the same time it might induce unexpected particle growth and surface morphology changes, resulting in altered ORR activity and stability.[7] Therefore, each catalyst has a different optimal heat-treatment temperature and time period. It was suggested that the presence of a second metal, such as Co, could increase the sintering resistance and prevent particle growth during heat treatments. As a result, the growth in PtCo particle size was slower than that of Pt particles.[77] Although there was evidence that the activity of the alloy catalyst could be affected by post-treatments,[69] possibly due to increased particle sizes and morphological changes, the Pt alloys after post-treatments still showed higher activity over the entire range of current densities than did Pt/C under identical conditions.[74]

Beside composition and post-treatment effects, other factors, for example the ordering structure of materials, may also affect catalytic activity and stability. It has been reported that an ordering structure was induced in some Pt alloys after heat treatments at high temperatures.[18,72] Xiong and Manthiram[59,78] reported that if PtCo/C or PtFe/C was heat-treated at 600–650 °C, a major transformation in ordering structure could be observed.

2.2.3 Effects of ordering. Many alloys, such as PtCr, PtCo, PtFe and PtV, can form ordered structures during synthesis or during heat treatment at high temperatures.[18,59,72,78] Unlike a disordered crystal structure, in which the two different types of atoms are randomly distributed, in an ordered structure they are arranged alternately, one on the other, to form a periodic superlattice structure. Alloys with ordered structures have yielded better specific catalytic activity than those with disordered structures, although the latter have exhibited greater stability.

Casado *et al.*[79] and Roychowdhury *et al.*[80] studied Pt-based ordered intermetallic compounds extensively and pointed out that these systems can provide predictable control over structural, geometric and electronic effects, while disordered structures cannot. While a disordered structure has varying local composition and atomic distribution, which may affect site activity, an ordered structure offers a consistent geometric and chemical environment, and thus the same activity. Ordered intermetallic phases with well-controlled geometric and electronic structures therefore may be promising avenues in the search for superior electrocatalysts for fuel cell applications.

Xiong and Manthiram[59,78] claimed that alloys with ordered structures might further enhance catalytic activity by

optimizing several factors, such as (i) the geometric and electronic structure of Pt, for the optimum number of base metal atoms as nearest neighbours, (ii) d-electron density in Pt atomic surface configuration, and (iii) Pt–Pt distance. In their study, the ordered structure was believed to be the reason for the higher activity in the PtFe/C and PtCo/C alloys compared to the PtNi/C and PtCu/C alloys, and also for the better activity in the ordered PtCo/C than in the disordered PtCo/C.

However, Watanabe *et al.*[72] carried out stability studies on both ordered and disordered PtCo/C catalysts, and observed up to 47% activity degradation in the ordered alloys, compared with only 1% degradation in the disordered alloys. Dissolution of cobalt from the ordered catalyst was several percentage points higher than from the disordered alloy, while new Pt phase formation occurred more quickly on the surface of the ordered alloy.

The effects of ordering might also depend on the specific components of Pt alloys. Antolini *et al.*[55] summarized the ordering effects of PtFe/C alloys reported from several groups.[81–83] For example, a PtFe/C alloy prepared by heat treatment at 750 °C and kept under flowing hydrogen for 12–15 h presented an ordered structure, and this ordered catalyst was found to be very stable when exposed to 0.5 M aqueous H_2SO_4. An insignificant amount ($\sim$0.6 ppm) of Fe was leached out during 16 h of testing, mainly from the free Fe ions present in the alloy. However, this result was opposite that obtained for PtCo/C alloy by Watanabe *et al.*[72]

2.2.4 Effects of the synthetic method. In synthesis, experimental conditions can significantly affect catalyst structures in terms of controlling morphology, shape and composition; crystalline structure; surface uniformity; the distribution of surface metals; and structural strength. Therefore, understanding these effects and using appropriate chemical protocols to optimize experimental conditions seem critical in obtaining highly active, stable nanostructured catalysts. Normally, synthesis of Pt alloys is performed by a solution-based (or chemical) method. Typically, such a synthesis uses precursors (usually a salt of the desired metals), a solvent, reducing agents, capping agents, and a medium that may affect the thermodynamics or kinetics of the reactions. By controlling one or more of the above-mentioned parameters, the desired products can be produced.

In the synthesis of conventional Pt-alloy nanoparticles, the main focus is on controlling the particle size, the degree of alloying, and the catalyst dispersion on the carbon support. The metal precursors and their concentrations have been proven to play critical roles in controlling product yields and particles sizes.[84] For example, adjusting the ratio between cobalt and platinum precursors (*i.e.*, increasing the concentration of cobalt in the reaction mixture) results in decreased Pt alloy particle size.[63,85,86]

It is recognized that adjusting precursor/capping agent concentrations and reduction/decomposition rates as well as selecting specific capping agents can control the morphology of nanostructures. A recent review article by Peng and Yang provided a fundamental understanding of the formation of Pt-alloy nanoparticles in solution phased synthesis.[87] From a thermodynamic point of view, the growth of an individual cluster is only favoured when it exceeds a critical size. In this article, the authors tabulated the effects of capping agents, solvents, reducing agents and additives when growing clusters with different sizes and morphologies. In particular, the authors pointed out that based on thermodynamic theory, stable nuclei should form in Pt-alloy nanoparticles that have smaller diameters than their pure metal counterparts.

The effects of capping agents on the morphology of nanoparticles have been well described for the synthesis of PtFe. Wang *et al.*[28] and Sun[88] synthesized PtFe nanoparticles with various morphologies—spheres, nanowires and nanorods—using simultaneously the reduction of platinum acetylacetonate ($Pt(acac)_2$) and the thermal decomposition of iron pentacarbonyl ($Fe(CO)_5$).[81,89] Synthesis was conducted under reflux in a mixture of oleylamine (OAm) and octadecene (ODE) at 160 °C. Dimensional control of the PtFe nanostructures was achieved by tuning the volume ratio of OAm to ODE. OAm, a common organic surfactant, is believed to have an elongated reverse-micelle-like structure and can effectively induce one-dimensional growth. The PtFe may have been nucleated inside this structure and surrounded by OAm with different packing densities in different directions, as illustrated by (1), (2) and (3) in Fig. 4.[28] The well-organized, dense molecular layers in direction (1) formed a hydrophobic barrier that prevented PtFe from being attached. In contrast, directions (2) and (3) had less densely packed OAm and therefore facilitated the growth of PtFe, resulting in the formation of nanowires or nanorods. A higher concentration of OAm relative to the precursors meant a plentiful supply of micellar structures to nurture nanowires, whereas diluting the OAm with ODE reduced the sizes of the structures, yielding nanorods. For example, PtFe nanowires over 200 nm long were obtained when OAm alone was used as both surfactant and solvent, while an OAm/ODE ratio of 3 : 1 yielded nanowires $\sim$100 nm long, and a 1 : 1 ratio produced nanorods 20 nm long. ODE may also affect growth; when a greater proportion of it was present (OAm : ODE = 1 : 3), the diameter of spherical PtFe nanoparticles could be controlled

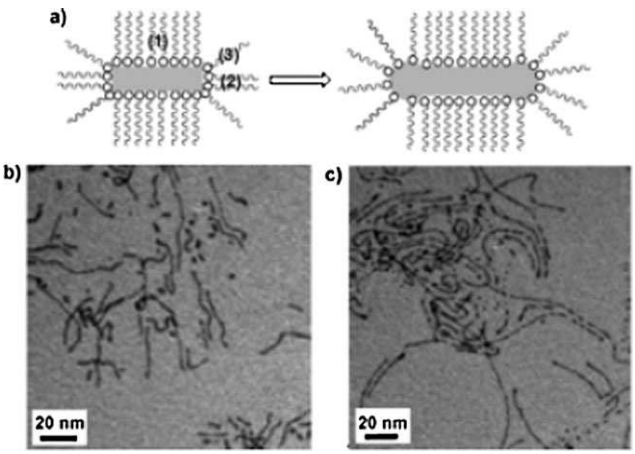

Fig. 4 (a) Schematic illustration of the growth mechanism of PtFe nanowires/nanorods, (b) TEM images of PtFe nanorods and (c) nanowires. (Reprinted from ref. 28 with permission by Wiley-VCH Verlag GmbH & Co. KGaA.)

at 3 nm. Interestingly, when an excess amount of $Fe(CO)_5$ was used in the reaction mixture, the product had less Fe content. The researchers also pointed out that PtCo nanowires could be made *via* the reduction of $Pt(acac)_2$ and the decomposition of $Co_2(CO)_8$ under similar reaction conditions. However, the resultant nanowires and nanorods were not thermally stable, as X-ray powder diffraction (XRD) measurements revealed. The authors suspected that during the annealing process, structures such as nanowires, which are more elongated, might have been more stable than nanorods. Researchers using similar approaches have also obtained uniform Pt nanorods and nanowires by adjusting the ratio of Pt precursor (*e.g.*, H_2PtCl_6) to sodium dodecyl sulfate in the polyol process.[90,91]

Ahmadi *et al.*[13] demonstrated that even using the same capping material, salt, temperature and solvent, changing only the ratio between the Pt ions and the capping material (sodium polyacrylate), the resulting products had differently shaped Pt nanoparticles. It was suggested that change in the concentration ratio could control the relative growth rate on {100} and {111}.

However, some drawbacks exist for capping agents, the major one being that poisoning of the catalyst surface thereby reduces the number of available catalytic sites. Lee *et al.*[92] compared the catalytic activities of Pt nanoparticle catalysts synthesized using poly(vinylpyrrolidone) (PVP) and tetradecyltrimethylammonium bromide (C_{14}TABr), as capping agents, and found that C_{14}TABr had a less poisonous effect than PVP in terms of catalytic activity.

2.3 Some issues

Using density functional theory (DFT) calculations, Nørskov *et al.*[33,93] provided insight into the effects of nanoparticle size on electrocatalytic activity. They concluded that these effects arose from strain induced at the nanoparticle surface, and varied with the thickness of the substrate. In Pt-alloys, Pt tends to congregate in the first layer and thus introduces surface strain, which strongly affects reactivity; the magnitude of the effect depends on the type of transition metal. Results showed that with increasing particle size, Au yielded a clear rise in catalytic rate per surface site, whereas Pt showed a decrease as particle size diminished. This difference was easily explained through a volcano-shaped dependency between electrocatalytic activity and the electronic state of the atoms.

It has been determined that base metal dissolution and leaching from Pt alloy catalysts are major issues for catalyst stability, particularly in a PEM fuel cell operating environment. Normally, most transition metals (such as Co, Cr, Fe, Ni, Mn, Cu and V) used as base metals in alloys are soluble at an electrode potential of 0.3–1 V *vs.* NHE in an acidic solution.[68] In the presence of a small amount of oxygen on the surface of nanosized PtM alloys, most transition metals will congregate on the surface,[6] which tends to be covered by base metal oxides such as Fe, Co and Ni that are easily oxidized.[16] Such a base metal oxide should dissolve easily in an acidic environment, resulting in more Pt on the catalyst surface.[55,72] The leaching of base-metal components into acidic ionomeric electrolyte has been suggested by Watanabe.[72] In a fuel cell MEA, if the base metal of an alloy catalyst in the catalyst layer were to leach into the ionomer and membrane, proton transfer within the catalyst layer and membrane would become difficult, resulting in degraded fuel cell performance. The dissolution of well-alloyed transition metals into the MEA after PEM fuel cell operation has been noted, using MEA cross-sectional analysis by the electron microprobe method.[77] The metal was dissolved from the alloy catalyst, and then it diffused into the membrane, which accounted for additional deterioration in long-term fuel cell performance.

Yu *et al.*[68] conducted extensive stability tests on PtCo/C cathode catalysts in a dynamic fuel cell environment with continuous water fluxing on the cathode. Dissolution of cobalt or platinum from the alloys was found to be the major cause of fuel cell degradation when the cathode was cycled for 400 cycles in the potential range of 0.87–1.2 V *versus* RHE.

Another major degradation mode could be changes in both the structure and the particle size of the alloy catalyst during PEM fuel cell operation. For example, researchers have observed a 20% increase in crystallite size, compared to an as-prepared catalyst, after repeated potential cycling measurements, indicating growth of the metal particles of the catalyst.[77] These structural changes and particle size increases may cause losses in fuel cell performance.

In summary, the activity and stability of Pt-alloy catalysts with a conventional spherical shape can be significantly affected by composition variation, post-treatments and crystalline structural changes. Composition may have more effect on catalytic activity, while the other factors may have greater effects on stability and durability. Unstable base metals (M) in PtM alloy catalysts can be dissolved or leached in an acidic fuel cell operation environment, causing first catalyst, then fuel cell degradation. It is expected that surface modification of Pt alloys with, for example, Pt-skins or surfaces textured with particular elements should be a promising way to address the issue of metal dissolution.

3. Nanotextured Pt alloys: Pt alloys covered by Pt-skin/monolayer

3.1 Current status—surface engineering strategies

Engineering Pt alloys to contain textured structures or dimensional elongation in a particular direction seems effective in improving catalytic activity and reducing dissolution of the base metal. Stamenkovic *et al.*,[9] for example, carried out extensive investigations on well-defined bulk PtNi and PtCo alloy surfaces, namely the Pt-skeleton surface and Pt-skin surface, and indicated that the ORR kinetics were dependent on the arrangement of alloying elements on the surface region. The catalytic activity at different surfaces was in the order of Pt_{bulk} < Pt-skeleton < Pt-skin. In their study of bulk $Pt_3Ni\{111\}$ catalyst with a crystal diameter of about 30 nm, they reported a ten-fold improvement in ORR activity compared to Pt{111} catalyst and a 90-fold greater activity than current state-of-the-art Pt/C catalysts for PEM fuel cells, making this, to date, the most active cathode catalyst that have been developed.[8] Roques *et al.*[74] theoretically studied Pt skins formed on the surface of Pt_3Co, Pt_3Cr and $Pt_{80}Fe_{20}$, and predicted that compared to a Pt{111} surface, the selectively

exposed $Pt_3Co\{111\}$ alloy surfaces could yield a 0.08 V positive potential shift for the formation of OH_{ads} from H_2O_{ads}. Similar results were confirmed using PtCr and PtFe alloys. It was concluded that the alloying process could modify the intrinsic catalytic activity when strong Pt–Cr and Pt–Co bonds were formed. This positive potential shift was also experimentally observed in a cyclic voltammetric measurement of PtCo/C catalyst at room temperature, which revealed that the ORR mechanism on such alloy surfaces was the same as that on a pure Pt surface, *i.e.*, a "series" four-electron reduction pathway.[94]

Adzic *et al.*[95] and Izzo[6] synthesized Pt monolayers on various core structures in an effort to stabilize Pt and Pt-group metals, as shown in Fig. 5.[96] Using either carbon-supported Pt or a noble single-crystal metal as the core (*e.g.*, a Pd nanoparticle or non-noble metal),[10,96] they deposited a monolayer of another noble metal on top of the substrate to form core–shell structured nanocatalysts, and tested for ORR activity and stability. Materials with this structure and various compositions have also been synthesized, achieving outstanding ORR activity. For example, in 0.1 M $HClO_4$ the Pt mass-specific activities for the ORR of Pt/Pd/C catalyst thus formed, with a typical loading of 3.4 $\mu g_{Pt}/cm^2$, were 5–8 times higher than that of Pt/C as measured with the rotating ring disk test. Using this catalyst, a four-electron ORR from O_2 to H_2O, with the first-charge transfer as the rate-determining step, was observed. A similar core–shell structure with a Pt monolayer on top of either Ir or Pd_3Co/C was also synthesized and tested for ORR activity and durability. When they were normalized according to Pt content, the two catalysts exhibited mass activities of 1.01 and 0.57 A mg^{-1}, respectively. These values exceeded the US Department of Energy (DOE) 2010 target of 0.44 A mg^{-1}. Durability tests showed that under a potential of 0 to 1.2 *vs.* RHE in 0.1 M $HClO_4$, the Pt/Pd_3Co/C core–shell structure had no apparent activity loss after 3000 cycles.[97]

Furthermore, in other approaches of Adzic *et al.*,[98] they deposited amorphous Au clusters onto carbon-supported Pt nanoparticles through galvanic replacement reactions, to improve stability. The resistance to dissolution of the Pt electrocatalyst was enhanced: after potential cycling between 0.6 and 1.1 V for over 30 000 cycles, no loss in ORR activity was observed.

In theoretical studies of the ORR mechanism catalyzed by PtM alloys, removal of adsorbed OH from the Pt surface is a major topic, because this removal is considered the rate-determining step in the overall ORR process. It has been realized that when alloying Pt with a metal such as Rh, Ir,

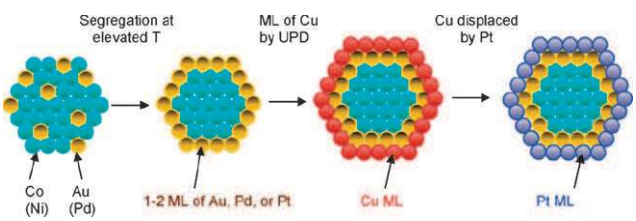

Fig. 5 Model for synthesis of Pt monolayer catalysts on non-noble metal–noble metal core–shell nanoparticles. (Adapted from ref. 96 with permission from American Chemical Society.)

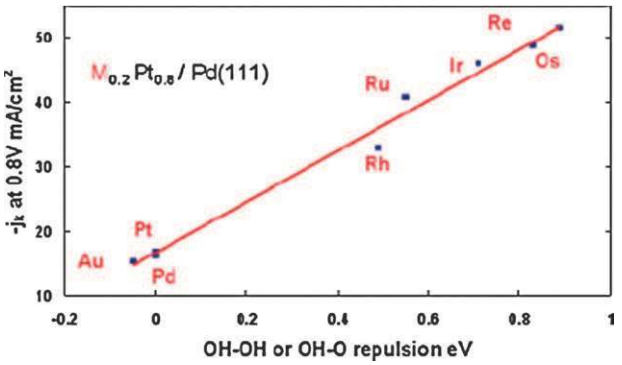

Fig. 6 Relationship between kinetic current at 0.80 V and the repulsive interaction in seven different $(Pt_3M)_{ML}$/Pd(111) (2 × 2) unit cells, compared to Pt_{ML}/Pd(111), characterized by the calculated interaction energy between two OH, or OH and O. (Reprinted from ref. 23 with permission from American Chemical Society.)

Ru, Os or Re, OH coverage of Pt can be reduced effectively, resulting in a faster ORR kinetics.[23] Fig. 6 shows a first-principle calculation of kinetic currents as a function of effective repulsion energy between two OHs, or between the O and OH, on a mixed PtM monolayer (M = Au, Pd, Rh, Ru, Ir, Re and Os) deposited on the Pd(111) surface. A linear correlation can be observed from this figure, indicating that reduced OH coverage on Pt was attributable to lateral repulsion between the adsorbed OH on Pt and the adsorbed OH or O on the neighbouring M metal atom. As a result, the kinetic current density for the ORR on this mixed PtM monolayer was found to be more than three times larger than on a pure Pt monolayer—this in addition to the fact that the ORR activity of such a Pt monolayer was already reportedly higher than that of pure Pt{111}. The oxidation of Pt in this mixed PtM monolayer was highly suppressed, only occurring at significantly higher potential (1.17 V).

3.2 Effects of composition, structure and morphology on ORR electrocatalyst performance

As discussed above, alloying Pt with base metals results in two key changes that may enhance the activity of these Pt alloy catalysts. First, alloying might change the electronic properties of platinum, and second, alloying with base metals may alter the adsorption properties of platinum. In addition, alloying could effectively reduce noble metal use and, thereby, overall cost. However, base metal dissolution leads to instability of Pt alloy catalysts, compromising the advantages of PtM alloys. This following section will review mitigation strategies for this issue.

Zhang *et al.*[10] engineered a functional monolayer on the surface of different core nanoparticles, and found that the electrochemical properties of the particles were dependent on the core composition and structures. For example, when a Pt monolayer was deposited on the surface of bulk Pd(111) single crystals,[10] the ORR activity, characterized using rotating ring disk electrode in a 0.1 M $HClO_4$ solution, revealed a very positive onset potential for the ORR (0.95–1 V *vs.* NHE), as well as a half-wave potential of 0.838 V. When such a Pt monolayer was deposited on the carbon-supported

Pd nanoparticles, even higher activity was observed, with a half-wave potential at 0.853 V. In addition, the ring current was insignificant, indicating that the ORR catalyzed by this catalyst was a complete four-electron process on the disk electrode from O_2 to H_2O. In their further studies, a Pt monolayer was also deposited on Au/Ni, Pd/Co and Pt/Co nanoparticles[96] to form core–shell Pt/Au/Ni, Pt/Pd/Co and Pt/Pt/Co nanoparticles, which were more active than Pt/C electrocatalyst. Fig. 7 presents a comparison of ORR activity on such core–shell electrocatalysts.[96] The polarization curves (left side of Fig. 7) were obtained using a rotating disk electrode (RDE) technique. The Pt mass activity and the total noble-metal mass activity (Pt plus the other noble metal) are expressed as currents at 0.85 and 0.80 V, respectively, on the right side of Fig. 7. The enhanced mass activity compared to that of commercially available Pt/C electrocatalyst was about 2.5 times for Pt and about 20 times for total noble metals (Pt + Pd), respectively. The high ORR activities of Pt monolayers on Au/Ni, Pd/Co and Pt/Co substrates were believed to arise from mismatching of the lattice constants between the monolayers and these substrates, as well as changes in the d-band properties of the Pt monolayer, caused by its interaction with the substrates. No anodic current was observed on the current–potential curves for oxidation/dissolution of Ni or Co, suggesting that the cores were covered by the Pt shells, and thus were inaccessible to the electrolyte solution.

A theoretic model was also constructed and applied to study the impact of different cores and Pt shells on catalytic activity;[6,99] conclusions indicated that the nature of the improved stability in such a core–shell structure also depended on the type of transition metal. For example, even when a small amount of oxygen was present on the surface, $Pt/Pd_3Co/C$ and Pt/Pd/C core–shell structures showed improved stability, while a $Pt/Pd_3Fe/C$ core–shell structure displayed decreased stability.

Modifying Pt/C particles with other metals may also prevent the oxidation of Pt. For example, if amorphous Au clusters are deposited on Pt/C nanoparticles, their stability may improve significantly.[98] Fig. 8 shows a stability comparison of ORRs catalyzed by Au-modified Pt/C (Au/Pt/C) and Pt/C catalysts in 0.1 M $HClO_4$ solution. Fig. 8 (right-hand) shows that after 30 000 cycles, there was no detectable loss of electrochemical Pt surface area (ECSA) on the Au/Pt/C catalyzed electrode, as compared with more than 45% loss of ECSA on the Pt/C electrode, even though the upper limit for the potential was not as high as for Au/Pt/C. For RDE measurements (left-hand of Fig. 8), there was only ~5 mV degradation in half-wave potential after the cycling period, compared to a 39 mV loss for Pt/C catalyst. Measurements by *in situ* X-ray absorption near edge spectroscopy (XANES) revealed that the strong d-orbital coupling between Pt and Au was induced by alloying, and could result in a lower surface energy or lower-lying Pt d-band states due to changes in electronic structures.

Koh and Strasser[11] reported significant activity enhancement of the ORR after Cu dealloying from carbon-supported Pt–Cu alloy nanoparticles. Their strategy was to modify a prepared carbon-supported Pt–Cu electrocatalyst by dealloying the non-noble metal Cu atoms from bimetallic precursors. After Cu atoms were removed from the surface region, the resulting catalyst particles showed core–shell structures and achieved a 4–6-fold improvement in ORR activity over that of pure Pt, as

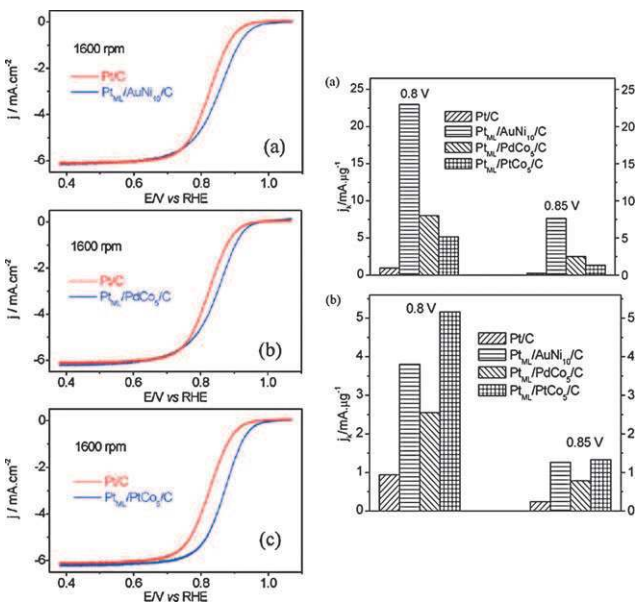

Fig. 7 (Left): Polarization curves for the ORR on carbon-supported Pt/Au/Ni, Pt/Pd/Co and Pt/Pt/Co core–shell nanoparticles in 0.1 M $HClO_4$, recorded at a potential sweep rate of 10 mV s^{-1} and room temperature. (Right): (a) Pt mass activity of different electrocatalysts; (b) total noble metal mass activity of different electrocatalysts. (Adapted from ref. 96 with permission from American Chemical Society.)

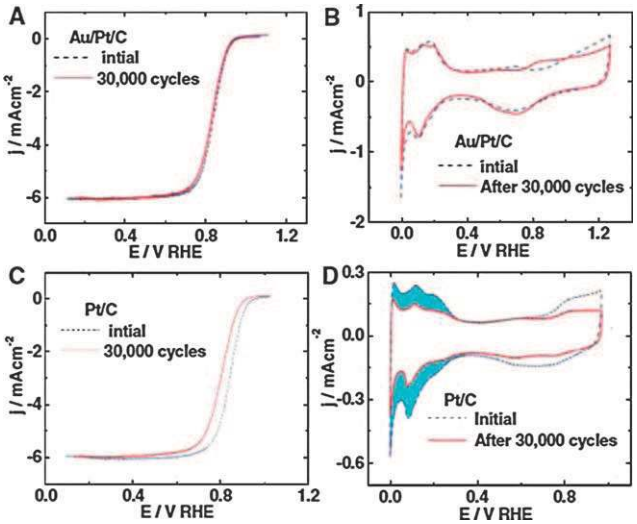

Fig. 8 Oxygen reduction reaction stability test on Au/Pt/C and Pt/C catalysts using a rotating disk electrode technique in 0.1 M $HClO_4$ at room temperature, before and after 30 000 potential cycles. Left: polarization curves Au/Pt/C (a) and Pt/C (c), recorded at a potential sweep rate of 10 mV s^{-1}; electrode rotation rate: 1600 rpm. Right: cyclic voltammetric curves for Au/Pt/C (b) and Pt/C (d), recorded at potential sweep rates of 50 and 20 mV s^{-1}, respectively. The shaded region in (d) indicates the lost Pt area. (Reprinted from ref. 98 with permission by the American Association for the Advancement of Science.)

confirmed by RDE tests with a Pt loading of 14 mg_{Pt} cm^{-2} at 0.9 V. Moreover, catalysts synthesized from a $Pt_{25}Cu_{75}$ precursor were also able to reach the 0.44 A mg^{-1}_{Pt} target set by the DOE for PEM fuel cell ORR catalysts. Stability testing for 4000 potential cycles between 0.6 and 1.0 V/RHE indicated that the dealloyed catalyst was able to maintain its activity over longer periods. Geometric effects were believed to be responsible for this activity enhancement after the Pt–Cu catalyst was dealloyed. Koh and Strasser also pointed out that dealloying might create favourable structural arrangements of Pt atoms on particle surfaces, forming more active crystallographic facets or more favourable Pt–Pt interatomic distances, both of which would benefit the ORR. Similar effects were also observed on carbon-supported Pt–Cu–Co ternary alloy nanoparticles with core–shell structures.[12]

Stamenkovic *et al.*[9,25,100] prepared Pt_3M (M = Co, Ni and Fe) with so-called "Pt-skin" bimetallic surfaces. Three different surfaces were obtained: (i) random surface, which consisted of randomly distributed Pt and M elements, (ii) Pt-skeleton surface, which consisted of 75 at.% Pt and 25 at.% M, obtained by sputtering and then treated by acid, and (iii) Pt-skin surface, which consisted of 100% Pt, prepared by high-temperature annealing. These three different surfaces all showed higher ORR activity in 0.1 M $HClO_4$ than in 0.5 M H_2SO_4. The Pt-skin surface on Pt_3Co exhibited the most enhanced activity in 0.1 M $HClO_4$, three to four times higher than for pure Pt, suggesting that a uniform monatomic layer of Pt surface atoms, with Pt depletion and Co enrichment in the second layer, has some unique catalytic properties. The enhanced activity was related to the formation of OH_{ad} at more positive potentials on the Pt-skin surface, induced by surface changes in the electronic structure. It has been recognized that Pt alloys covered by a Pt skin are an effective means of improving ORR activity and stability. The enhancement order seems to be: Pt-skin > Pt-skeleton > pure Pt-polycrystalline structure.

Further study by Stamenkovic *et al.*[8] led to remarkable progress in new ORR catalyst development. They introduced $Pt_3Ni\{111\}$, a single-crystal catalyst that showed 10 times higher mass activity (TOF of 2800 e $site^{-1}$ s^{-1}) than current state-of-the art Pt/C in 0.1 M $HClO_4$ solution. For their catalyst, they identified the three outermost layers: the innermost of these was Pt-enriched, with a Pt content of 87%; the middle atomic layer was Ni-enriched, with 52% Ni; and the outer layer contained almost 100% Pt. They also showed that different low-index surfaces on this PtNi alloy had different ORR activities. The ORR activity order was identified as: $Pt_3Ni\{100\}$-skin < $Pt_3Ni\{110\}$-skin < $Pt_3Ni\{111\}$-skin, as shown in Fig. 9. The unusually high catalytic activity of $Pt_3Ni\{111\}$ was attributed to low OH_{ad} coverage during the ORR, induced by altered electronic surface properties after alloying. In similar research, Roques *et al.*[74] conducted some theoretical calculations for the Pt skin structure that covers the topmost layers of PtM{111} (M = Co, Cr and Fe). The proposed model for PtCo{111} showed that the surface Pt could offer at least two different Pt sites with different coordination number. These two Pt sites exhibited different adsorption properties for both OH and H_2O. Relative to the Pt{111} surface, a positive potential shift in reversible

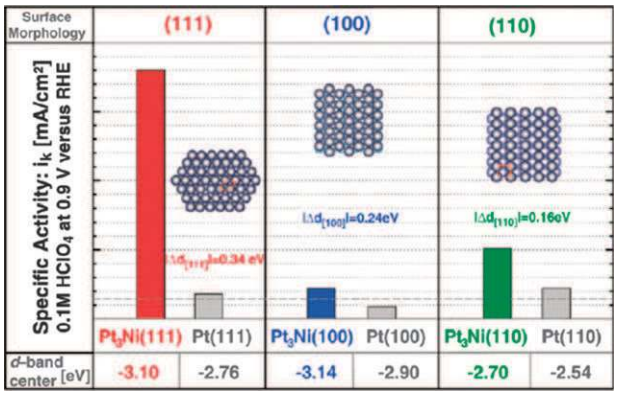

Fig. 9 Kinetic current density i_k, measured at 0.9 V *vs.* RHE on $Pt_3Ni(hkl)$ surfaces, in comparison to the corresponding Pt(*hkl*) surfaces (a horizontal dashed gray line marks the specific activity of polycrystalline Pt), to show the influence of surface morphology and electronic surface properties on the kinetics of ORR measurements in 0.1 M $HClO_4$ at room temperature with 1600 rpm. (Reprinted from ref. 8 with permission by the American Association for the Advancement of Science.)

potential could be predicted based on their model, calculated for the formation of OH_{ads} from H_2O_{ads} on the Pt skin; this was confirmed experimentally using PtCo/C catalyst.

3.3 Effects of the synthetic method

Baumgärtner and Raub[101] in 1988 reviewed the work to-date on electrodeposition methods for fabricating platinum and some platinum alloys. PtM (M = Pd, Co, Ni, Cu, Zn, Cd, Sn, Ru, Ir and Re) alloys could be synthesized using this method. Their review extensively explored the effects of electrolyte, platinum salts and current density.

Zhang *et al.*[10,23,96,98] synthesized core–shell structured PtM nanoparticles using galvanic displacement underpotential deposition (UPD), as shown in Fig. 5.[96] By this method, a mixed monolayer containing Pt, Au or PtM (M = Au, Pd, Rh, Ru, Ir, Re and Os) was deposited on the surfaces of single-crystal or carbon-supported nanoparticles. For example, in the synthesis of surface-modified Pt nanoparticles using Au-clusters, a Cu monolayer was first applied to carbon-supported Pt nanoparticles by underpotential deposition, and an Au adlayer was then deposited through galvanic replacement, resulting in replacement of the Cu monolayer by the Au adlayer. The Au adlayer was further cooked by voltammetric cycling (10 cycles) between 0.2 and 1.2 V *vs.* RHE with a potential sweep rate of 50 mV s^{-1}, to obtain the Au clusters. CO stripping measurements on Au/Pt/C found 30–40% coverage of Au clusters on the Pt surface, and high-resolution transmission electron microscopy revealed that most exposed Pt facets on the Au/Pt/C assembly were Pt{111}, while the Au clusters appeared to be in an amorphous phase (Fig. 10).[98] Electrodeposition of Pt onto a $RuO_2(110)$ single crystal surface was reported by the same group.[102]

As discussed above, Koh and Strasser[11] reported a synthetic strategy that seemed to be effective in modifying the surface reactivity of Pt and Pt-alloys; this was a two-step process, involving preparation of carbon-supported Cu-rich precursor alloys followed by electrochemical dissolution of Cu (dealloying).

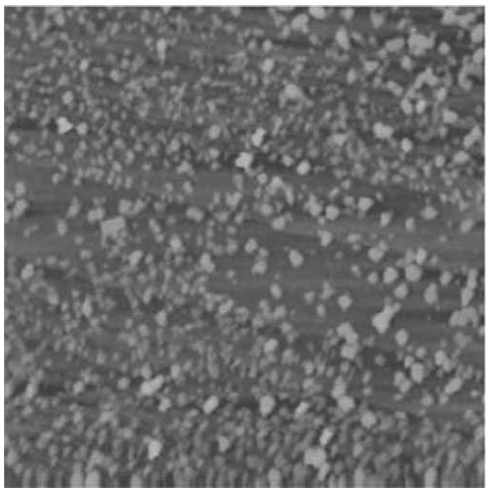

Fig. 10 STM image (125 × 125 nm) of the Au clusters on a Pt(111) surface. (Image was acquired at an electrode potential of 0.8 V in 0.1 M $HClO_4$ at room temperature; the tunneling current was 1.24 nA.) (Reprinted from ref. 98 with permission by the American Association for the Advancement of Science.)

X-Ray diffraction measurements indicated that Cu and Pt atoms could form disordered Pt–Cu alloy phases that had reduced Pt–Pt interatomic distances, with subsequent selective electrochemical dissolution of Cu believed to be the key process in the formation of an active catalyst. Energy dispersive X-ray spectroscopy and X-ray photoelectron spectroscopy revealed a core–shell structure with Pt-enriched Pt–Cu alloy ($Pt_{79}Cu_{21}$) as the core and an essentially pure Pt surface ($Pt_{93}Cu_7$) as the shell. These results suggested that surface dealloying might be a useful synthetic strategy to tune the surface catalytic properties of noble metal catalysts.

Hetero-epitaxial growth has also been employed to produce various core–shell Pt alloy nanostructures in the solution phase. Habas *et al.*[103] reported a well-defined core–shell Pt/Pd structure synthesized using preformed Pt nanocubes as seeds for nucleation. Since the lattice mismatch between Pd and Pt is very small (only 0.77%), the preformed, well-defined Pd shape could also be used as a seed for epitaxial growth with Pt, to form a thin uniform Pt shell on the surface of the Pd core. AuPt core–shell structures have been produced by a similar approach using Au nanorods as seeds.[103]

Carbon-supported Pd-rich pseudo-core–shell Pd–Pt (Pd@Pt/C) nanoparticles can be prepared by a galvanic replacement reaction, and analyzed using microstructural characterization techniques.[104] Core–shell $Pd_{70}@Pt_{30}$ catalysts with a loading of 20.4 μg (total metals) per cm^2 showed a minimum two-fold enhancement in their ORR activity in 0.1 M $HClO_4$, and presented some advantages in terms of cost and methanol tolerance.

In summary, Pt alloys with a surface engineering strategy have shown promise in improving catalytic activity and stability. However, one concern is that preparing such Pt alloys requires some complicated processing procedures and post-treatments. Another concern is that the larger spherical particle size of these Pt alloys (> 9 nm)—much larger than the optimal size of *ca.* 4 nm for the ORR—is usually a result of this strategy, and could be further optimized.[7] It is believed that catalysts developed using this strategy should be validated in a fuel cell operating environment to assess long-term stability.

4. Branched or anisotropic elongated Pt and Pt-alloy nanostructures—morphology and shape-controlled Pt-based catalysts

4.1 Current status—dimensional strategies

In general, "nanostructure" refers to a material with at least one dimension in the range of 1–100 nm.[15] In recent years, nanostructures with different shapes, such as spheres, wires, rod, whisks and tubes, have been explored as electrocatalysts in PEM fuel cell applications, and have demonstrated significantly enhanced catalytic activity and selectivity for the ORR.[15,28,105]

Lim *et al.* reported successful synthesis of branched Pt multi-octahedrons[106] and Pd–Pt nanodendrites[107] with a high ratio of {111} to {100} as exposed facets. This catalyst exhibited a higher catalytic activity than commercially available Pt/C (*E*-TEK) catalyst. Fig. 11 shows a half-wave potential of 0.843 obtained from 20 nm Pt multi-octahedrons[106] in O_2-saturated 0.1 M $HClO_4$ solution, using the rotating disk electrode (RDE) test; this result was slightly higher than the 0.840 V obtained for Pt/C baseline catalyst, and the multi-octahedra specific activity was almost three times higher than that of Pt/C. In addition, the Pt and Pt-alloy catalysts were also significantly more stable. For example, a stability test of the Pt multi-octahedra catalyst over 4000 potential cycles, in an 0.1 M $HClO_4$ solution in the potential range of 0.6–1.1 V *vs.* RHE, showed a slight loss of 5.7% in electrochemical surface area (ECSA), while a 34% ECSA loss was observed for Pt/C catalyst under the same testing conditions.[106] In addition, after the stability test, the branched structure of this catalyst was

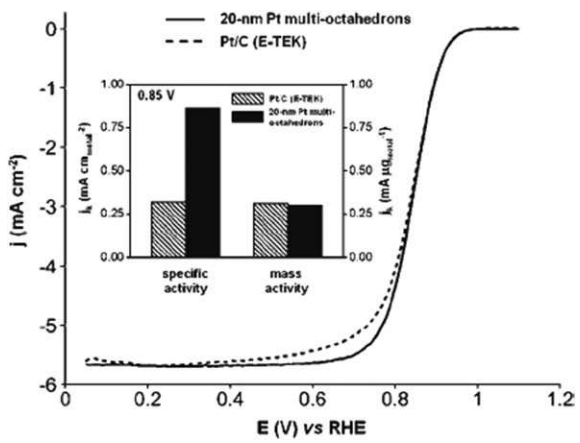

Fig. 11 Polarization curves for ORR performance on 20 nm Pt multi-octahedra and Pt/C (*E*-TEK) catalysts, recorded at room temperature with a sweep rate of 10 mV s^{-1} in O_2-saturated 0.1 M $HClO_4$ solution. The inset compares the specific activity (left) and mass activity (right) for these two catalysts at 0.85 V. The kinetic currents were calculated using mass-transport correction from ORR polarization curves. The loadings of 20 nm Pt multi-octahedrons and Pt/C (*E*-TEK) catalyst on the rotating disk electrode were both 15 μg_{Pt} cm^{-2}. (Adapted from ref. 106 with permission from American Chemical Society.)

retained without significant particle coarsening. This might be the reason for the stability of the catalyst.

Hollow structures with at least one nanoscaled dimension (*i.e.*, 1–100 μm) could combine both advantages of the dimensions and high space utilizations, and offer a uniquely high surface area compared to their solid counterparts. Chen *et al.*[26] reported on the synthesis of supportless Pt and PtPd nanotubes (PtNTs and PtPdNTs) and the use of these as electrocatalysts for the ORR. Some improvements in both activity and stability were observed. The stability test, conducted with 1000 potential cycles in a potential range of 0 to 1.3 V *vs.* RHE in Ar-purged 0.5 M H_2SO_4 solution at 60 °C, revealed only ~20% loss in ECSA for PtNTs and PtPdNTs, compared to ~90% ECSA loss for a Pt/C catalyst, as shown in Fig. 12. Furthermore, no noticeable morphological changes were observed in the PtNTs and PtPdNTs after this stability test. The enhanced ORR activity of the PtNT and PtPdNT catalysts was attributed to the preferential exposure of certain crystal facets. Success in the synthesis of Pt and Pt-alloy nanowires, nanorods and nanotubes may herald a new direction in the fabrication of freestanding electrodes for PEM fuel cell applications.

Alternatively, a new class of Pt nanostructures, for example, the branched Pt nanoparticles that include nanostars, nanoarms and nanopods, have also been explored as ORR catalysts for fuel cell applications.[108] These nanostructures can be synthesized using chemical methods under carefully controlled experimental conditions. Some special nanoparticle shapes, such as cubic, truncated cubic and plate-like, can also be formed.[15,16,37,85] By extending the dimension of nanoparticles in a desired direction, some well-defined, so-called one-dimensional nanostructures such as nanotubes, nanowires, nanobelts, nanoneedles and nanorods have been synthesized, and these exhibit enhanced ORR catalytic activity and selectivity.[15,28]

Apparently, we need systematic studies of controlling parameters in the synthetic routes of Pt nanostructures with different shapes—such as spheres, wires, rods, whiskers and tubes—for application in electrochemical energy devices.

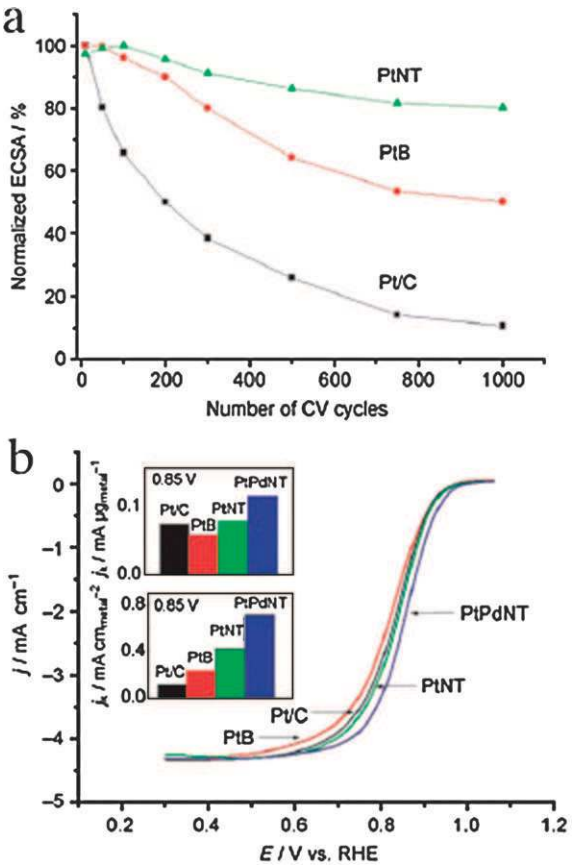

Fig. 12 (a) Comparison study of the loss of electrochemical Pt surface area (ECSA) of Pt/C (*E*-TEK), platinum-black (PtB; *E*-TEK), and PtNT catalysts with a number of CV cycles in Ar-purged 0.5 M H_2SO_4 solution at 60 °C (0–1.3 V *vs.* RHE, sweep rate 50 mV s^{-1}). (b) Polarization curves of Pt/C, platinum black (PtB), PtNTs and PdPtNTs for ORR performed in O_2-saturated 0.5 M H_2SO_4 solution at room temperature (1600 rpm, sweep rate 5 mV s^{-1}). Inset: Mass activity (top) and specific activity (bottom) for the four catalysts at 0.85 V. (Reprinted from ref. 26 with permission by Wiley-VCH Verlag GmbH & Co. KGaA.)

4.2 Developments of the synthetic method

Xia *et al.* in 2003 published a comprehensive review of one-dimensional[15] and shape-controlled[16] metal nanostructures, looking at synthetic methods and mechanisms, catalyst characterization, and applications. In their review, they extensively examined strategies for obtaining dimensional nanostructures by anisotropic growth; the use of appropriate reduction agents and capping reagents; and the effects of ion spectators. They found that reaction temperature, ionic species and reaction environment could change the reaction pathway in precursor reduction or decomposition, and then control the morphology of metal nanostructures. The crystal growth pathway can be changed thermodynamically and kinetically when different mediators are used in a synthetic environment.[109,110]

Regarding kinetic and thermodynamic control of the synthesis process, several factors should be considered, including: (i) reduction rate of precursors, (ii) nucleation rate on the sites, (iii) surface energy of individual facets, and (iv) reaction temperature. Depending on the use of different metal precursors, reducing agents, capping agents, and other species as mediators in the reaction solution, these four factors may be significantly affected. Normally, typical reducing reactants are alcohols, glycols and hydrazines.[88] In a so-called polyol process, a diol or polyalcohol (for example, ethylene glycol) may also be used as the reducing agent to reduce metal salts to metal particles. Ethylene glycol has been identified as unique in serving as both the solvent and the primary reductant for Pt nanocrystal synthesis.[16,111,112] It has also been recognized that the kinetics of crystal growth can be controlled by reducing agents. For example, a strong reducing agent may assist in the formation of thermodynamically favoured polyhedral nanocrystals.[113] A mild reducing agent might block or slow down the growth site in one direction and promote overgrowth in others, facilitating the anisotropic growth that forms whiskers, nanopods, or nanostars. For example, by using $NaBH_4$ to reduce K_2PtCl_4, Pt nanocubes were formed.[38] However, if a milder reducing agent such as ascorbic acid was used, Pt nanodendrites were produced.[114,115]

Thermodynamic control can be achieved by altering the surface energy of prepared materials. Species such as O_2, CO, H^+, OH^-, and some ions, such as Fe^{2+} or Fe^{3+} and Br^-, might play important roles in changing the rates of reduction and growth in different crystallographic planes. These species could selectively change the surface affinity towards specific crystal facets or chemisorptions, resulting in a morphology change in the nanocrystals.[111] For example, the presence of Br^- was found to reduce the surface energy of {100} facets, leading to controlled growth ratio between exposed {111} and {100}. The same approach was also used to affect the growth rate of nucleation along the ⟨100⟩ axis by adding Ag^+ into the reaction solution.[116] Sea-urchin-shaped Pt nanostructures were obtained by a polyol process in air at 110 °C,[90] with the help of a trace amount of Fe^{2+} (or Fe^{3+}) in the solution to control the thermodynamics and kinetics of the reduction reaction. The other examples for such controlling synthesis are the formation of Pt nanotetrapods,[117] Pt nanowires (Fig. 13(a)),[90] and nanoflowers (Fig. 13(b)),[106] by adding Fe^{3+} or gaseous species such as N_2 or H_2 into the reaction solutions.

As stated above, the highly branched Pt multi-octahedra[106] and Pd–Pt nanodendrites,[114] with highly exposed facet ratios of {111} to {100}, exhibited higher catalytic activity and stability than commercially available Pt/C catalyst. In addition, the unsupported Pt and PtPd nanotubes (PtNTs and PtPdNTs)[26] displayed enhanced ORR activity and stability when used as electrocatalysts. Driven by the promising ORR performance of such catalysts, researchers have recently accelerated their work on morphology and shape-controlled Pt-based catalysts.

Chen *et al*. reported that Pt nanostructures in the form of spheres, star-shaped particles, branched multipods and nanowires could be synthesized by controlling the reduction kinetics of a polyol process. Four-armed Pt nanostructures were obtained *via* this chemical route (Fig. 14(a)) and identified by high-resolution TEM as having a single-crystalline structure (Fig. 14(b)).[117] By controlling the concentration of Pt precursors and the synthesis time, researchers have grown the arms of the Pt nanopods into straight nanowires along the ⟨111⟩ direction (Fig. 14(d)), to a length greater than 500 nm (Fig. 14(c)).[90,91]

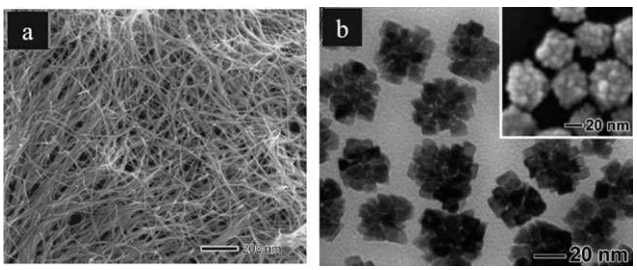

Fig. 13 (a) SEM image showing a magnified view of long Pt nanowires. (Adapted from ref. 91 with permission by Wiley-VCH Verlag GmbH & Co. KGaA.) (b) TEM and scanning electron microscopy (SEM) (inset) images of Pt nanoflowers, obtained in the presence of a trace amount of iron species. (Adapted from ref. 106 with permission from American Chemical Society.)

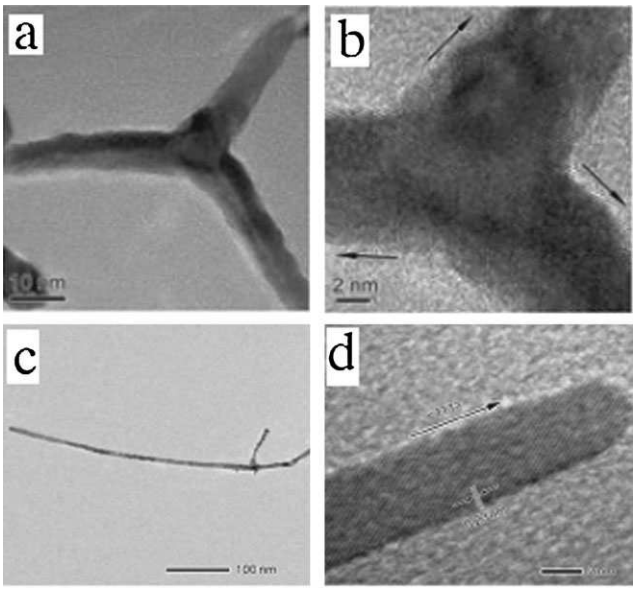

Fig. 14 (a) TEM and (b) HRTEM images of the four-armed Pt nanostructures, showing a single-crystal structure. (Adapted from ref. 117 with permission by Wiley-VCH Verlag GmbH & Co. KGaA.) (c) TEM image of an individual Pt nanowire 5 nm in diameter and more than 500 nm in length. (d) HRTEM image of the tip of an individual single crystal Pt nanowire grown along the ⟨111⟩ axis. (Adapted from ref. 91 with permission by Wiley-VCH Verlag GmbH & Co. KGaA.)

Sun *et al*. reported a simple room-temperature, aqueous-phase synthesis of single-crystal Pt nanowires on nanospheres of carbon black. The Pt nanostructures were confirmed as having single-crystalline structures, and the arms were grown along the ⟨111⟩ direction.[118] By adjusting the weight ratio of Pt precursor to carbon, the coverage of Pt nanowires on the surface of the carbon nanoparticles was controlled (Fig. 15).[119]

The anisotropic morphology of preformed seeds could lead to the formation of branched Pt nanostructures through non-symmetrical growth.[15] Using preformed nanostructures as seeds, well-defined core–shell structures, nanowires and nanotubes were synthesized.[16,96,98] Mahmoud *et al*.[47] employed tetrahedral Pt as seeds to fabricate star-like Pt nanostructures with up to thirty arms, as shown in Fig. 16.

For Pt-alloy nanowires, Wang *et al*.[28] were successful in controlling the length of Pt–Fe nanowires and nanorods during synthesis, by adjusting the volume ratio of oleylamine to octadecene. The obtained PtFe nanowires were 200 nm in length and ~2–3 nm in diameter.

Shui *et al*.[105] used the electrospinning method to synthesize long (up to cm) Pt nanowires with a diameter of a few nanometres. The purpose was to make a freestanding fuel cell electrode from these nanowires. The experimental setup, as shown in Fig. 17, consisted of a high-voltage supplier, a syringe pump, and a plastic syringe equipped with a 22-gauge stainless steel needle. Carbon paper was used to collect the composite nanowires. They also studied the effects of polymer PVP concentration, precursor H_2PtCl_6 concentration, water content in the solvent, electric field strength, and feeding rate on the morphology of the resultant nanowires. In a typical experiment to make a uniform nanowire structure without

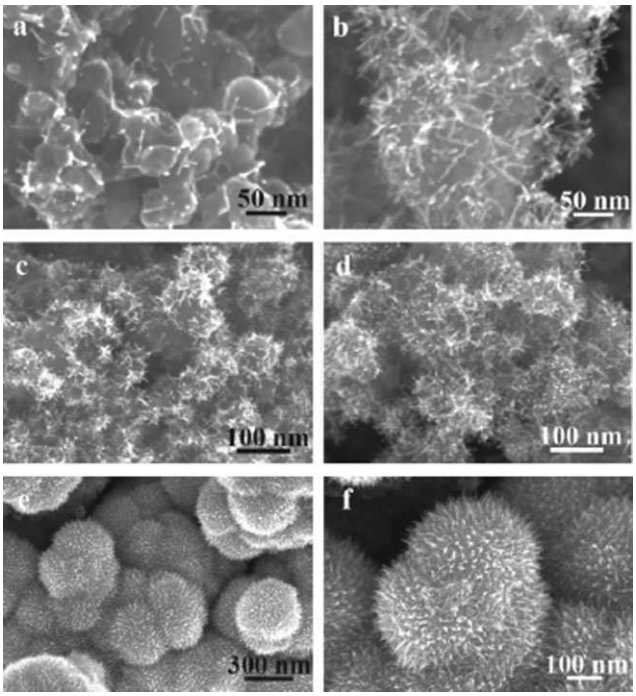

Fig. 15 (a–f) SEM micrographs showing the evolution of Pt nanowire coverage on carbon nanospheres, controlled by the weight ratio of Pt to carbon. (Reprinted from ref. 119 with permission by Wiley-VCH Verlag GmbH & Co. KGaA.)

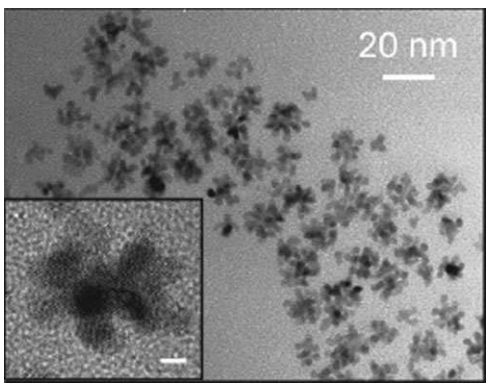

Fig. 16 TEM image of multi-armed Pt nanoparticles, with an HRTEM image (inset) displaying multiple arms branching in various directions from the initial seed particle. The scale bar in the inset is 2 nm. (Reprinted from ref. 47 with permission from American Chemical Society.)

beads, PVP and H_2PtCl_6 are used as the capping agent and Pt precursor, respectively, as shown in Fig. 18.

Core–sheath nanofibers with a broad range of diameters and sheath thicknesses can also be fabricated using a modified electrospinning method.[120–123] In a typical synthesis, the ethanol solution containing the sol–gel precursors, the reducing agent and capping agent is loaded in the outer capillary while a heavy mineral oil is added to the inner capillary. The core–sheath nanofibers can be made hollow by extracting the mineral oil using a solvent that can be removed with post-treatments. By selectively modifying the oil core with different precursors, and using outer surfaces

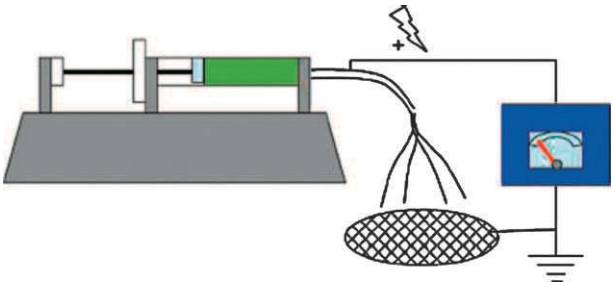

Fig. 17 Setup of electrospinning apparatus for fabrication of nanowires. (Reprinted from ref. 105 with permission from American Chemical Society.)

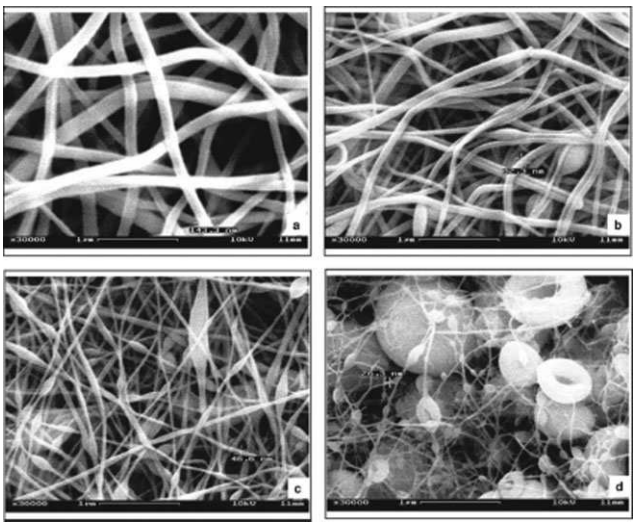

Fig. 18 Effect of PVP concentrations (a) 35, (b) 24.5, (c) 17.5 and (d) 10.5 mg ml^{-1}, on the morphology of Pt nanowires fabricated by the electrospinning technique. (Reprinted from ref. 105 with permission from American Chemical Society.)

composed of composite and ceramic, hollow nanofibers can be selectively modified according to the requirements for different applications.

Template-engaged replacement reactions (TERR) have been demonstrated to be effective in generating hollow nanostructures of noble metals, including Pt nanotubes and nanoshells with homogeneous and highly crystalline walls.[27,124,125] In synthesis, the template surface (*e.g.*, the channel in a porous membrane, nanowire, or colloidal particle) may be directly coated with a metal monolayer to produce a core–shell nanostructure.

Mayers *et al.*[27] employed trigonal selenium (t-Se) nanowires and amorphous selenium (a-Se) spherical colloids as both chemical and physical templates to form Pt hollow nanotubes with controllable shape, size and wall thickness, as shown in Fig. 19(a). Using $PtCl_2$ as a precursor, they obtained Pt nanotubes by coating the surfaces of t-Se nanowires with Pt at 50 °C for 18 h in an ethanol solution. After Pt coating, the Se template was removed either by soaking the sample in pure hydrazine monohydrate liquid for 5 h, or by thermal evaporation by heating the dried sample on a hotplate at 200–250 °C for a few minutes. In this way, Pt nanotubes with a uniform wall thickness of 9 ± 2 nm and a diameter of 2–4 nm were

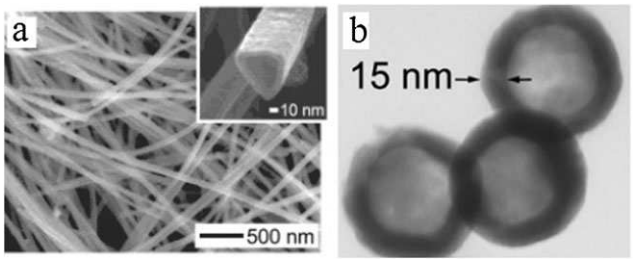

Fig. 19 (a) SEM images of Pt nanotubes using Se as template. (b) TEM of Se@Pt core–shell colloids with uniform shells formed on the surface of a Se core. (Adapted from ref. 27 with permission from American Chemical Society.)

produced. It is believed that two successive reduction reactions were involved in the process: the Pt^{2+} salt was first reduced by the Se template at the interface through galvanic reduction, then further reduced by alcohol solvent. The reduction process was controlled by time or Pt^{2+} salt concentration, forming Pt nanotubes or nanoshells with various thicknesses. When the spherical colloid of amorphous selenium (a-Se) was used as a template, uniform core–shell colloids (Se@Pt) were obtained, as shown in Fig. 19(b).

In the process of template synthesis combined with the galvanic replacement reaction, template metals are required to reduce precursor metal ions in the solution. Pt, PtAg and PtPd nanotubes have been successfully synthesized using silver nanowires as the template, because the standard reduction potential of a Pt^{2+}/Pt pair (1.2 V *vs.* SHE) is higher than that of a Ag^{+}/Ag pair (0.80 V *vs.* SHE).[26,124,126,127] In this synthesis, silver nanowires suspended in the solution were oxidized by $Pt(CH_3COO)_2$ according to the following replacement reaction:

$$Pt(CH_3COO)_2\,(aq) + 2Ag\,(s) \rightarrow Pt\,(s) + 2Ag(CH_3COO)\,(aq) \quad (1)$$

Since both silver and platinum have a face-centered cubic lattice, and their lattice parameters are very similar (3.92 and 4.0862 Å for platinum and silver, respectively), the resulting Pt atoms tend to be epitaxially deposited on the surface of the Ag template. After the Ag template was partially consumed, PtAg alloy is formed on the surface of the Ag template, and through an Ostwald ripening process, a smooth and seamless shell is eventually generated. In a similar approach, Ag and Cu nanowires have been used as a template to generate Au (Fig. 20),[128] Pd and Pt nanotubes through a galvanic replacement reaction.

Using biological molecules such as the Tobacco Mosaic Virus (TMV) as templates, some nanowires of PtCo, Pt_3Co and Pt_3Fe alloys have been successfully synthesized.[129] This study showed that the presence of both Co^{2+} and Pt^{2+} ions inside TMV channels was necessary for nanowire formation. In this process, $NaBH_4$ was required for the reduction process. It was also observed that the growth of the nanowires inside the TMV central channels could be boosted by ultrasonication.

As demonstrated above, alongside the methods chosen for catalyst synthesis, some other factors, such as reducing agent, capping agent, ion spectators, and seeds also play significant roles in obtaining nanostructures with controlled shapes.

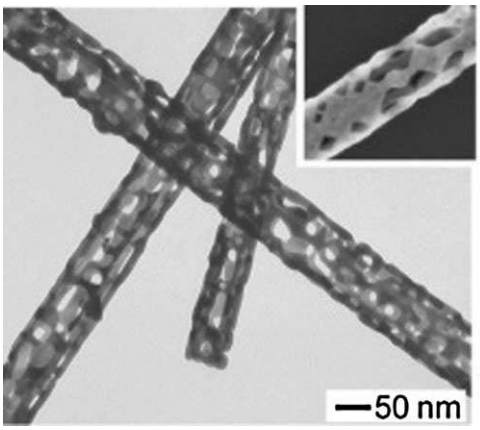

Fig. 20 TEM image of Au nanotubes with porous walls. The inset is an SEM image of the corresponding sample. (Reprinted from ref. 128 with permission from American Chemical Society.)

5. Conclusion and outlook

Under the strong driving force of fuel cell commercialization, great progress in PEM fuel cell catalysis has been made in the last two decades. At the present time, the most practical catalysts for fuel cell applications are still Pt-based catalysts, such as carbon-supported Pt and Pt–Ru alloy catalysts. In this article, achievements and major challenges, including (for the latter) high cost, insufficient activities and low stability, have been reviewed, and technological developments for addressing these challenges in recent years discussed, with a focus on developing functional, nanostructured Pt-alloy catalysts.

The nanostructured Pt alloy catalysts developed for PEM fuel cell reactions can be grouped into different clusters: (i) Pt-alloy nanoparticles, (ii) Pt-alloy nanotextures such as Pt-skins/monolayers on the top of base metals, and (iii) branched or dimensional Pt or Pt-alloy nanostructures. It was demonstrated that advanced alloy nanostructures showed great potential in solving issues of insufficient activity and low stability, by combining the advantages of dimensions and large surface area. For example, the recently developed Au nanotubes featured with porous walls look very promising, as shown in Fig. 20.[128] Pt-containing catalysts with such a structure could be a new class of self-supported catalysts to avoid problems of use of carbon supports and particle growth by Ostwald ripening. Scheme 1 shows the evolution of Pt-based catalysts and future directions for improvements through the engineering of structure and composition. All three groups of Pt-alloy electrocatalysts present unique advantages. In the case of nanoparticles, size is the dominant parameter for optimizing activity and can easily be controlled. The optimal size for electrocatalytic activity is in the range of $\sim$4 nm, or around 10 unit cells of Pt lattice. When a lattice consists of polycrystals, some boundary effects and strains arise from improper fitting. Pt-alloy nanoparticles with a single crystalline structure, on the other hand, have a relatively dense structure and fewer surface defects; this leads to much greater stability, but sites for electrocatalytic activity may need to be created.

One-dimensional nanostructured Pt-alloys offer better stability and durability, while textured Pt-skins/monolayers

may enhance activity and stability. Combining the features of these three structural groups—for example, nanotubes with porous walls to increase the volume-to-face ratio—may be a good approach to improve catalytic activity and stability. Other factors, such as ion transport and the design of MEAs for practical fuel cell applications, should be considered.

Although some Pt alloy catalysts with advanced nanostructures have shown remarkable activity, the dissolution of metals, including Pt and alloyed base metals, in fuel cell operation environments could cause catalyst degradation, which still remains an issue. Another issue may be the low retention of active catalyst nanostructure during fuel cell operation. For example, the crystal facets that contain more catalytically active sites could be converted to a low active facet due to thermodynamic environmental changes in the fuel cell processing. The nanosized Pt alloy catalysts still face the instability of Ostwald ripening. All these issues will result in the degradation of catalytic activity and stability. Furthermore, for Pt-alloys with core–shell and elongated nanostructures, scale-up synthesis and fuel cell testing beyond RDE experiments is challenging.

At the nanoscale level, the effects of surface properties—including physical and chemical properties such as surface area, electronic structure, atomic arrangement and defects—on electrocatalytic activity are much stronger than at micro- or macroscale levels. Some theories may have to be revised to accommodate the mechanisms of electrocatalytic activity in nanoscale materials.

It seems there are no clear answers about the dominant factors in catalyst activity enhancement and this area should be an on-going research topic in catalyst development. Based on our understanding, the extent to which such nanostructured Pt-alloys enhance catalyst activity and stability is strongly dependent on geometric and electronic effects, as well as on the type of transition metal in the Pt-alloy. Composition appears to be very important in modifying the surface structure of Pt-alloys. Other factors, such as size, shape and morphology, are also instrumental in varying the number of active sites and stabilizing the surface structure, as well as preventing metal dissolution.

Additional approaches to reducing the cost of catalysts for the ORR include other replacements for Pt-based catalysts. For example, a new class of low-cost, non-precious metal catalysts have been synthesized and are reported to be promising for use as high-activity ORR catalysts.[2,130]

Future work should focus on the following aspects: (i) optimizing the geometry, composition and structure of Pt alloys to further improve their catalytic activity and stability; (ii) validating the activity and stability of these remarkable catalysts using real fuel cell operating conditions—these nanostructured catalysts have shown excellent activity and stability in electrochemical cell measurements; (iii) further exploring new catalyst morphologies to resolve the issue of low retention in highly active nanostructures; this low retention is caused by fuel cell operation; (iv) developing self-supported nanostructured catalysts to avoid the problems of carbon supports and particle growth by Ostwald ripening; and (v) developing cost-effective catalyst synthesis processes to meet the requirements for fuel cell commercialization.

Acknowledgements

The authors would like to thank the Institute for Fuel Cell Innovation, National Research Council of Canada, for its financial support.

References

1 L. Garland Nancy, in *Fuel Cell*, 2008 DOE Hydrogen Program Merit Review and Peer Evaluation Meeting, Arlington, Washington, DC, 2008.
2 R. Bashyam and P. Zelenay, *Nature*, 2006, **443**, 63.
3 H. A. Gasteiger, S. S. Kocha, B. Sompalli and F. T. Wagner, *Appl. Catal., B*, 2005, **56**, 9.
4 A. S. Aricoò, P. Bruce, B. Scrosati, J. M. Tarascon and W. van Schalkwijk, *Nat. Mater.*, 2005, **4**, 366.
5 H. Liu, D. Xia and J. Zhang, in *PEM Fuel Cell Electrocatalysts and Catalyst Layers: Fundamentals and Applications*, ed. J. Zhang, Springer, New York, 2008, ch. 13, p. 631.
6 A. E. Izzo, *Highly Dispersed Alloy Cathode Catalyst for Durability*, 2008 Progress Report for the DOE Hydrogen Program focuses on fuel cells, Washington, DC, 2008.
7 E. Antolini, *J. Mater. Sci.*, 2003, **38**, 2995.
8 V. R. Stamenkovic, B. Fowler, B. S. Mun, G. Wang, P. N. Ross, C. A. Lucas and N. M. Markovic, *Science*, 2007, **315**, 493.
9 V. Stamenkovic, T. J. Schmidt, P. N. Ross and N. M. Markovic, *J. Phys. Chem. B*, 2002, **106**, 11970.
10 J. Zhang, Y. Mo, M. B. Vukmirovic, R. Klie, K. Sasaki and R. R. Adzic, *J. Phys. Chem. B*, 2004, **108**, 10955.
11 S. Koh and P. Strasser, *J. Am. Chem. Soc.*, 2007, **129**, 12624.
12 R. Srivastava, P. Mani, N. Hahn and P. Strasser, *Angew. Chem., Int. Ed.*, 2007, **46**, 8988.
13 T. S. Ahmadi, Z. L. Wang, T. C. Green, A. Henglein and M. A. El-Sayed, *Science*, 1996, **272**, 1924.
14 C. Burda, X. Chen, R. Narayanan and M. A. El-Sayed, *Chem. Rev.*, 2005, **105**, 1025.
15 Y. Xia, P. Yang, Y. Sun, Y. Wu, B. Mayers, B. Gates, Y. Yin, F. Kim and H. Yan, *Adv. Mater.*, 2003, **15**, 353.
16 Y. Xia, Y. Xiong, B. Lim and S. E. Skrabalak, *Angew. Chem., Int. Ed.*, 2009, **48**, 60.
17 E. Antolini, *Appl. Catal., B*, 2007, **74**, 324.
18 B. C. Beard and J. Ross, *J. Electrochem. Soc.*, 1990, **137**, 3368.
19 S. Mukerjee, S. Srinivasan, M. P. Soriaga and J. McBreen, *J. Electrochem. Soc.*, 1995, **142**, 1409.
20 M. T. Paffett, J. G. Beery and S. Gottesfeld, *J. Electrochem. Soc.*, 1988, **135**, 1431.
21 T. Toda, H. Igarashi, H. Uchida and M. Watanabe, *J. Electrochem. Soc.*, 1999, **146**, 3750.
22 S. Zhou, K. McIlwrath, G. Jackson and B. Eichhorn, *J. Am. Chem. Soc.*, 2006, **128**, 1780.
23 J. Zhang, M. B. Vukmirovic, K. Sasaki, A. U. Nilekar, M. Mavrikakis and R. R. Adzic, *J. Am. Chem. Soc.*, 2005, **127**, 12480.
24 S. Alayoglu, A. U. Nilekar, M. Mavrikakis and B. Eichhorn, *Nat. Mater.*, 2008, **7**, 333.
25 V. R. Stamenkovic, B. S. Mun, M. Arenz, K. J. J. Mayrhofer, C. A. Lucas, G. Wang, P. N. Ross and N. M. Markovic, *Nat. Mater.*, 2007, **6**, 241.
26 Z. Chen, M. Waje, W. Li and Y. Yan, *Angew. Chem., Int. Ed.*, 2007, **46**, 4060.
27 B. Mayers, X. Jiang, D. Sunderland, B. Cattle and Y. Xia, *J. Am. Chem. Soc.*, 2003, **125**, 13364.
28 C. Wang, Y. Hou, J. Kim and S. Sun, *Angew. Chem., Int. Ed.*, 2007, **46**, 6333.
29 H. A. Gasteiger and M. Nenad, *Science*, 2009, **324**, 48.
30 J. S. Filhol and M. Neurock, *Angew. Chem., Int. Ed.*, 2006, **45**, 402.
31 M. J. Janik, C. D. Taylor and M. Neurock, *J. Electrochem. Soc.*, 2009, 156.
32 M. Neurock, M. J. Janik, S. A. Wasileski, A. Anderson and S. Mukerjee, *Insights into the overpotential for oxygen reduction on Pt and Pt skin alloys: A comparison of theory and experiment*, 2005 AIChE Annual Meeting and Fall Showcase, October 30, 2005. Conference Proceedings, Cincinnati, OH, p. 10621.

33 J. K. Nørskov, T. Bligaard, B. Hvolbæk, F. Bild-Pedersen, I. Chorkendorff and C. H. Christensen, *Chem. Soc. Rev.*, 2008, **37**, 2163.
34 V. Stamenkovic, B. S. Mun, K. J. J. Mayrhofer, P. N. Ross, N. M. Markovic, J. Rossmeisl, J. Greeley and J. K. Nørskov, *Angew. Chem., Int. Ed.*, 2006, **45**, 2897.
35 J. K. Nørskov, J. Rossmeisl, A. Logadottir, L. Lindqvist, J. R. Kitchin, T. Bligaard and H. Jónsson, *J. Phys. Chem. B*, 2004, **108**, 17886.
36 Z. L. Wang, *J. Phys. Chem. B*, 2000, **104**, 1153.
37 J. Chen, B. Lim, E. P. Lee and Y. Xia, *Nano Today*, 2009, **4**, 81.
38 K. M. Bratlie, H. Lee, K. Komvopoulos, P. Yang and G. A. Somorjai, *Nano Lett.*, 2007, **7**, 3097.
39 A. Kuzume, E. Herrero and J. M. Feliu, *J. Electroanal. Chem.*, 2007, **599**, 333.
40 M. D. Maciá, J. M. Campiña, E. Herrero and J. M. Feliu, *J. Electroanal. Chem.*, 2004, **564**, 141.
41 N. M. Markovic, H. A. Gasteiger and J. Ross, *J. Phys. Chem.*, 1995, **99**, 3411.
42 P. Zelenay, M. Gamboa-Aldeco, G. Horányi and A. Wieckowski, *J. Electroanal. Chem.*, 1993, **357**, 307.
43 K. Varga, P. Zelenay and A. Wieckowski, *J. Electroanal. Chem.*, 1992, **330**, 453.
44 M. E. Gamboa-Aldeco, E. Herrero, P. S. Zelenay and A. Wieckowski, *J. Electroanal. Chem.*, 1993, **348**, 451.
45 D. Armand and J. Clavilier, *J. Electroanal. Chem.*, 1989, **270**, 331.
46 D. Armand and J. Clavilier, *J. Electroanal. Chem.*, 1989, **263**, 109.
47 M. A. Mahmoud, C. E. Tabor, M. A. El-Sayed, Y. Ding and L. W. Zhong, *J. Am. Chem. Soc.*, 2008, **130**, 4590.
48 G. C. Bond, *Platinum Met. Rev.*, 1975, **19**, 126.
49 G. A. Somorjai and D. W. Blakely, *Nature*, 1975, **258**, 580.
50 C. Wang, H. Daimon, T. Onodera, T. Koda and S. Sun, *Angew. Chem., Int. Ed.*, 2008, **47**, 3588.
51 N. Markovic, H. Gasteiger and P. N. Ross, *J. Electrochem. Soc.*, 1997, **144**, 1591.
52 R. Narayanan and M. A. El-Sayed, *J. Phys. Chem. B*, 2005, **109**, 12663.
53 N. Tian, Z. Y. Zhou, S. G. Sun, Y. Ding and L. W. Zhong, *Science*, 2007, **316**, 732.
54 S. Mukerjee and S. Srinivasan, *J. Electroanal. Chem.*, 1993, **357**, 201.
55 E. Antolini, J. R. C. Salgado and E. R. Gonzalez, *J. Power Sources*, 2006, **160**, 957.
56 B. S. Mun, M. Watanabe, M. Rossi, V. Stamenkovic, N. M. Markovic and J. Ross, *J. Chem. Phys.*, 2005, **123**, 204717.
57 S. Mukerjee, S. Srinivasan, M. P. Soriaga and J. McBreen, *J. Phys. Chem.*, 1995, **99**, 4577.
58 Y. S. Lee, J. Y. Rhee, C. N. Whang and Y. P. Lee, *Phys. Rev. B: Condens. Matter Mater. Phys.*, 2003, **68**, 235111.
59 L. Xiong and A. Manthiram, *J. Electrochem. Soc.*, 2005, **152**, A697.
60 P. B. Balbuena, D. Altomare, N. Vadlamani, S. Bingi, L. A. Agapito and J. M. Seminario, *J. Phys. Chem. A*, 2004, **108**, 6378.
61 H. Yano, M. Kataoka, H. Yamashita, H. Uchida and M. Watanabe, *Langmuir*, 2007, **23**, 6438.
62 H. R. Colon-Mercado, H. Kim and B. N. Popov, *Electrochem. Commun.*, 2004, **6**, 795.
63 H. R. Colon-Mercado and B. N. Popov, *J. Power Sources*, 2006, **155**, 253.
64 X. Li, H. R. Colon-Mercado, G. Wu, J. W. Lee and B. N. Popov, *Electrochem. Solid-State Lett.*, 2007, **10**, B201.
65 M. T. Paffett, K. A. Daube, S. Gottesfeld and C. T. Campbell, *J. Electroanal. Chem.*, 1987, **220**, 269.
66 J. Luo, P. N. Njoki, Y. Lin, L. Wang and C. J. Zhong, *Electrochem. Commun.*, 2006, **8**, 581.
67 T. Ioroi and K. Yasuda, *J. Electrochem. Soc.*, 2005, **152**, A1917.
68 P. Yu, M. Pemberton and P. Plasse, *J. Power Sources*, 2005, **144**, 11.
69 S. C. Ball, S. L. Hudson, J. H. Leung, A. E. Russell, D. Thompsett and B. R. C. Theobald, *ECS Trans.*, 2007, **11**, 1247.
70 S. C. Ball, B. Theobald, D. Thompsett and S. Hudson, *ECS Trans.*, 2006, **1**, 141.
71 A. Bonakdarpour, J. Wenzel, D. A. Stevens, S. Sheng, T. L. Monchesky, R. Lobel, R. T. Atanasoski, A. K. Schmoeckel, G. D. Vernstrom, M. K. Debe and J. R. Dahn, *J. Electrochem. Soc.*, 2005, **152**, A61.
72 M. Watanabe, K. Tsurumi, T. Mizukami, T. Nakamura and P. Stonehart, *J. Electrochem. Soc.*, 1994, **141**, 2659.
73 E. Antolini, J. R. C. Salgado and E. R. Gonzalez, *Appl. Catal., B*, 2006, **63**, 137.
74 J. Roques, A. B. Anderson, V. S. Murthi and S. Mukerjee, *J. Electrochem. Soc.*, 2005, **152**, E193.
75 L. Zhang, K. Lee and J. Zhang, *Electrochim. Acta*, 2007, **52**, 3088.
76 C. W. B. Bezerra, L. Zhang, H. Liu, K. Lee, A. L. B. Marques, E. P. Marques, H. Wang and J. Zhang, *J. Power Sources*, 2007, **173**, 891.
77 S. C. Zignani, E. Antolini and E. R. Gonzalez, *J. Power Sources*, 2008, **182**, 83.
78 L. Xiong and A. Manthiram, *J. Mater. Chem.*, 2004, **14**, 1454.
79 E. Casado-Rivera, D. J. Volpe, L. Alden, C. Lind, C. Downie, T. Vazquez-Alvarez, A. C. D. Angelo, F. J. DiSalvo and H. D. Abruna, *J. Am. Chem. Soc.*, 2004, **126**, 4043.
80 C. Roychowdhury, F. Matsumoto, V. B. Zeldovich, S. C. Warren, P. F. Mutolo, M. Ballesteros, U. Wiesner, H. D. Abruna and F. J. DiSalvo, *Chem. Mater.*, 2006, **18**, 3365.
81 S. Sun, C. B. Murray, D. Weller, L. Folks and A. Moser, *Science*, 2000, **287**, 1989.
82 A. K. Shukla, M. Neergat, P. Bera, V. Jayaram and M. S. Hegde, *J. Electroanal. Chem.*, 2001, **504**, 111.
83 A. K. Shukla, R. K. Raman, N. A. Choudhury, K. R. Priolkar, P. R. Sarode, S. Emura and R. Kumashiro, *J. Electroanal. Chem.*, 2004, **563**, 181.
84 M. Jitianu, R. Kleisinger, M. Lopez and D. V. Goia, *J. New Mater. Electrochem. Syst.*, 2007, **10**, 67.
85 E. V. Shevchenko, D. V. Talapin, H. Schnablegger, A. Kornowski, O. Festin, P. Svedlindh, M. Haase and H. Weller, *J. Am. Chem. Soc.*, 2003, **125**, 9090.
86 J. R. C. Salgado, E. Antolini and E. R. Gonzalez, *J. Phys. Chem. B*, 2004, **108**, 17767.
87 Z. Peng and H. Yang, *Nano Today*, 2009, **4**, 143.
88 S. Sun, *Adv. Mater.*, 2006, **18**, 393.
89 M. Chen, J. P. Liu and S. Sun, *J. Am. Chem. Soc.*, 2004, **126**, 8394.
90 J. Chen, T. Herricks, M. Geissler and Y. Xia, *J. Am. Chem. Soc.*, 2004, **126**, 10854.
91 J. Chen, Y. Xiong, Y. Yin and Y. Xia, *Small*, 2006, **2**, 1340.
92 H. Lee, S. E. Habas, S. Kweskin, D. Butcher, G. A. Somorjai and P. Yang, *Angew. Chem., Int. Ed.*, 2006, **45**, 7824.
93 J. Meier, J. Schiøtz, P. Liu, J. K. Nørskov and U. Stimming, *Chem. Phys. Lett.*, 2004, **390**, 440.
94 J. Roques and A. B. Anderson, *Surf. Sci.*, 2005, **581**, 105.
95 R. R. Adzic, J. Zhang, K. Sasaki, M. B. Vukmirovic, M. Shao, J. X. Wang, A. U. Nilekar, M. Mavrikakis, J. A. Valerio and F. Uribe, *Top. Catal.*, 2007, **46**, 249.
96 J. Zhang, F. H. B. Lima, M. H. Shao, K. Sasaki, J. X. Wang, J. Hanson and R. R. Adzic, *J. Phys. Chem. B*, 2005, **109**, 22701.
97 S. Motupally, 2008 DOE Hydrogen Program Merit Review and Peer Evaluation Meeting, Arlington, Washington, DC, 2008.
98 J. Zhang, K. Sasaki, E. Sutter and R. R. Adzic, *Science*, 2007, **315**, 220.
99 G. E. Ramirez-Caballero and P. B. Balbuena, *Chem. Phys. Lett.*, 2008, **456**, 64.
100 V. R. Stamenkovic, B. S. Mun, K. J. J. Mayrhofer, P. N. Ross and N. M. Markovic, *J. Am. Chem. Soc.*, 2006, **128**, 8813.
101 M. E. Baumgartner and Ch. J. Raub, *Platinum Met. Rev.*, 1988, **32**, 188.
102 M. B. Vukmirovic, P. Liu, J. T. Muckerman and R. R. Adzic, *J. Phys. Chem. C*, 2007, **111**, 15306.
103 S. E. Habas, H. Lee, V. Radmilovic, G. A. Somorjai and P. Yang, *Nat. Mater.*, 2007, **6**, 692.
104 J. Yang, J. Y. Lee, Q. Zhang, W. Zhou and Z. Liu, *J. Electrochem. Soc.*, 2008, **155**, B776.
105 J. Shui and J. C. M. Li, *Nano Lett.*, 2009, **9**, 1307.
106 B. Lim, X. Lu, M. Jiang, P. H. Camargo, E. C. Cho, E. P. Lee and Y. Xia, *Nano Lett.*, 2008, **8**, 4043.
107 B. Lim, M. Jiang, P. H. C. Camargo, E. C. Cho, J. Tao, X. Lu, Y. Zhu and Y. Xia, *Science*, 2009, **324**, 1302.
108 N. C. Bagkar, H. M. Chen, H. Parab and R.-S. Liu, in *Electrocatalysis of Direct Methanol Fuel cells*, ed. H. Liu and J. Zhang, WILEY-VCH, Weinheim, Germany, 2009, ch. 2.

109 V. F. Puntes, K. M. Krishnan and P. Alivisatos, *Appl. Phys. Lett*., 2001, **78**, 2187.
110 V. F. Puntes, K. M. Krishnan and A. P. Alivisatos, *Science*, 2001, **291**, 2115.
111 Y. Xiong, J. M. McLellan, J. Chen, Y. Yin, Z. Y. Li and Y. Xia, *J. Am. Chem. Soc*., 2005, **127**, 17118.
112 B. Veisz and Z. Király, *Langmuir*, 2003, **19**, 4817.
113 L. Zhang, K. Lee and J. Zhang, *Electrochim. Acta*, 2007, **52**, 7964.
114 B. Lim, M. Jiang, P. H. C. Camargo, E. C. Cho, J. Tao, X. Lu, Y. Zhu and Y. Xia, *Science*, 2009, **324**, 1302.
115 Y. Song, Y. Yang, C. J. Medforth, E. Pereira, A. K. Singh, H. Xu, Y. Jiang, C. J. Brinker, F. Van Swol and J. A. Shelnutt, *J. Am. Chem. Soc*., 2004, **126**, 635.
116 H. Song, F. Kim, S. Connor, G. A. Somorjai and P. Yang, *J. Phys. Chem. B*, 2005, **109**, 188.
117 J. Chen, T. Herricks and Y. Xia, *Angew. Chem., Int. Ed*., 2005, **44**, 2589.
118 S. Sun, D. Yang, D. Villers, G. Zhang, E. Sacher and J. P. Dodelet, *Adv. Mater*., 2008, **20**, 571.
119 S. Sun, F. Jaouen and J. P. Dodelet, *Adv. Mater*., 2008, **20**, 3900.
120 G. Larsen, R. Velarde-Ortiz, K. Minchow, A. Barrero and I. G. Loscertales, *J. Am. Chem. Soc*., 2003, **125**, 1154.
121 D. Li and Y. Xia, *Nano Lett*., 2004, **4**, 933.
122 D. Li, J. T. McCann and Y. Xia, *Small*, 2005, **1**, 83.
123 I. G. Loscertales, A. Barrero, I. Guerrero, R. Cortijo, M. Marquez and A. M. Ganan-Calvo, *Science*, 2002, **295**, 1695.
124 Y. Sun, B. T. Mayers and Y. Xia, *Nano Lett*., 2002, **2**, 481.
125 Y. Sun and Y. Xia, *Nano Lett*., 2003, **3**, 1569.
126 Y. Bi and G. Lu, *Chem. Mater*., 2008, **20**, 1224.
127 Y. Sun and Y. Xia, *Synthesis and Characterization of Metal Nanostructures with Hollow Interiors*, Department of Chemistry, University of Washington, Seattle, WA, 2003.
128 Y. Sun and Y. Xia, *J. Am. Chem. Soc*., 2004, **126**, 3892.
129 R. Tsukamoto, M. Muraoka, M. Seki, H. Tabata and I. Yamashita, *Chem. Mater*., 2007, **19**, 2389.
130 M. Lefevre, E. Proietti, F. Jaouen and J. P. Dodelet, *Science*, 2009, **324**, 71.

